PHILOSOPHICAL TRANSACTIONS OF THE ROYAL SOCIETY A MATHEMATICAL, PHYSICAL & ENGINEERING SCIENCES

Water Movement in Wet Snow

J. M. N. T. Gray

Phil. Trans. R. Soc. Lond. A 1996 **354**, 465-500
doi: 10.1098/rsta.1996.0017

Water movement in wet snow

By J. M. N. T. Gray†

School of Mathematics, University of East Anglia, Norwich NR4 7TJ, UK

Contents

The three phases of water co-exist at the triple-point temperature which is very close to 273.1 K. Wet snow packs are therefore nearly isothermal. Weak temperature gradients result from the dependence of the triple-point on grain size and capillary pressure and these need to be considered if metamorphism of the snow pack is modelled. The bulk energy balance determines the amount of latent heat released by phase change that is necessary to maintain the triple-point temperature. Solar radiation occurring on diurnal timescales generates significant amounts of melt water in a surface layer and the subsequent unsaturated flow, as the water percolates down through the pack under the action of gravity, is governed by the theory of immiscible displacement. This introduces a partitioning of the water into an immobile, or bound, phase, which is trapped in the necks of the grain boundaries, and a mobile phase. The theory of interacting continua (mixture theory) provides a natural framework in which to describe all these processes and the necessary assumptions are discussed in detail for a four constituent snow pack consisting of ice, mobile water, bound water and air. Earlier work has suggested that the capillary pressure is proportional to the reciprocal of the mobile water saturation; however, the experimental data on which this is based is sparse and there are equally likely functional forms with more realistic behaviour. The most notable problem with the existing capillary pressure is that it is unbounded in the limit as the saturation tends to zero. A physically realistic

† Present address: Institute für Mechanik, Technische Hochschule Darmstadt, 64289 Darmstadt, Germany.

Phil. Trans. R. Soc. Lond. A (1996) **354**, 465–500
Printed in Great Britain

model can not support infinite pressures as these would produce infinite forces in the momentum balance and drive unbounded flows. Current water percolation models only work because the relative permeability fortuitously introduces another singularity that controls the limit behaviour. While this does not present a problem when used in isolation, it will produce unbounded rates of mass supply and unbounded temperatures in wet snow metamorphism models that include phase change and the triple-point dependence on capillary pressure, which is clearly physically unsatisfactory. A simple modification in which the capillary pressure remains bounded is not sufficient to eradicate these problems and must be supplemented by a relative permeability which has a finite gradient at zero saturation to obtain physically realistic results. This introduces a creep state in which water continues to flow, however low the saturation becomes, not present with the power law relative permeability used in current models. Complete drainage of the snow pack in finite time can only occur if the creep state model is used. Four combinations of the capillary pressure and relative permeability functions are investigated to demonstrate that these changes have a significant effect on the nature of the solution. Scaling arguments are used to draw out the balances in the equations and determine the appropriate magnitudes of the saturation, velocity, and time and length scales for each class. At low water fluxes the length and timescales of the flows are those suggested by the diurnal forcing. However, for larger fluxes the nonlinear nature of the equations cause a front to develop whose time and length scales are ten times shorter than the corresponding diurnal scales. The water mass and momentum balances can be combined to obtain a nonlinear diffusion equation for the saturation, whose diffusion coefficient is given by the relative permeability multiplied by the capillary pressure gradient with respect to saturation. Travelling wave solutions are constructed for each of the four classes which provide a useful check on numerical methods. If the diffusion coefficient equals zero at zero saturation, then the saturation equation has a degenerate form which admits the possibility of solutions with a discontinuous derivative. Numerical methods which can solve more general problems are developed for both non-degenerate and degenerate cases. Finally, numerical illustrations are presented for a simple forcing scenario in which the saturation varies sinusoidally on the diurnal timescale at the surface.

1. Introduction

Water run-off from seasonal snow covers and melting glaciers is very important to the hydrological cycle in cold regions. Many months of surface accumulation can be stored within a snow pack which may lead to a shortage of water for agriculture, domestic use and electricity generation, while too much run-off during rapid ablation may present the risk of flooding. In addition, while most land ice is below freezing throughout the year, a rise in mean temperature associated with global warming could induce or enhance melting in the surface snow layers and this melt may ultimately contribute to sea level rise. The understanding of the flow of water through a snow pack after it melts in the surface layers is central to the ability to forecast run-off hydrographs. The unsaturated flow is fully three-dimensional, and is complicated further by the presence of ice layers and inhomogeneities in the ice matrix which lead to routing through drainage channels and fingering. Two comprehensive reviews on the general subject area are given by Wankiewicz (1978) and Gray (1980).

PHILOSOPHICAL TRANSACTIONS OF THE ROYAL SOCIETY A MATHEMATICAL, PHYSICAL & ENGINEERING SCIENCES

One-dimensional models have been developed to describe these complex flows in some approximate mean sense. The simplest theory which ignores the diffusive effects of capillary pressure (Colbeck 1971, 1972, 1977), assumes that the relative permeability has a power law dependence on saturation with real exponent $n > 1$. The saturation equation following from this gravity flow theory has a hyperbolic structure which supports nonlinear waves. These are well understood (e.g. Whitham 1974). Regions of higher saturation move faster and, therefore, catch up with regions of lower saturation ahead of them, distorting the wave profile until ultimately the wave breaks and becomes triple valued. Weak solutions which support jump discontinuities can then be constructed by shock fitting. Drainage tests were used by Colbeck & Davidson (1973) to determine that the exponent $n \simeq 3.3$. When capillary pressures are introduced into the basic gravity flow theory (Colbeck 1974) the saturation equation is parabolic and the diffusion smooths out discontinuities, so the shock fronts are replaced by continuous sharp wave fronts. Analysis of these more complex systems are extremely limited, although Colbeck (1974) found an approximate solution valid at the wave front. Numerical methods are the only way of obtaining practical solutions to more general problems (e.g. Jordan 1991).

This paper presents a comprehensive discussion of the one-dimensional movement of water in snow in which the effects of capillary pressure are included. The analysis starts with the underlying framework of mixture theory and discusses the constitutive postulates necessary to construct a closed system of equations. One of the main points to emerge from this formal derivation is that as the saturation tends to zero the capillary pressure relation, suggested in the work of Colbeck (1974), becomes unbounded. A physically realistic model can not support infinite pressures as these would produce infinite forces in the momentum balance and drive unbounded flows. In Colbeck's (1974) theory (which is uncoupled from the thermodynamics) this works because the relative permeability fortuitously introduces another singularity that controls the limit behaviour. However, when wet snow metamorphism (Colbeck 1973, 1975, 1982, 1987) is included the triple-point temperature (at which ice and water coexist) is proportional to the capillary pressure and also becomes unbounded, which is clearly physically unsatisfactory. A forecasting model which seeks to model both water movement and metamorphism in wet snow (e.g. Morris & Godfrey 1978) will run into severe difficulties at low saturation. Alternatively, if the triple-point pressure dependence is re-interpreted; or if the temperature is simply assumed to be isothermal at the outset, then the pressure working terms in the energy balance for the snow become large at low saturation, and consequently large phase change terms enter the saturation equation, which violate the assumptions of the uncoupled model. The experimental data on which the capillary pressure dependence on saturation is based (Colbeck 1974) is sparse, and there are alternative functional forms which fit the data at least as well. This paper investigates the effects of different model assumptions. In particular, if the existing snow metamorphism theory stands, then the capillary pressure must have a finite upper bound and the relative permeability relation must have a finite gradient at zero saturation.

2. Mixture framework

The theory of interacting continua (mixtures) provides a rational mathematical framework in which to describe a phase changing snow pack. A general model consists of four constituents (Morland *et al.* 1990), namely the three phases of water (ice,

PHILOSOPHICAL TRANSACTIONS OF THE ROYAL SOCIETY A MATHEMATICAL, PHYSICAL & ENGINEERING SCIENCES

liquid water, water vapour) and air. Reduced models appropriate to *dry* sub-freezing snow, where liquid water is absent, have been investigated in detail by Gray & Morland (1994) and Gray *et al.* (1995). Here we formulate the basic mixture relations and conservation laws for a *wet* snow pack.

In general, wet snow is unsaturated and the motion of the liquid water and the air is governed by the theory of immiscible displacement (Bear 1972). It is conventional to decompose the water component into two parts. A mobile phase, which is free to percolate through the snow, and an immobile or bound phase, which is trapped in the necks of the grain boundaries and does not move relative to the ice. Typically between 2 and 7% of the pore space is occupied by immobile water in fully drained snow packs and it is assumed that the same proportion of water, the *irreducible water saturation* $S_{\rm wi}$, remains bound even when mobile water is flowing over it.

For simplicity the water vapour is neglected here, leaving again a four-constituent theory, composed of ice, mobile water, bound water, and air (referred to by the labels $\nu = \mathrm{i}, \mathrm{w}, \mathrm{b}, \mathrm{a}$). Each constituent ν occupies a volume fraction, ϕ^ν, per unit mixture volume and by definition these volume fractions lie between zero and one and their sum equals unity:

$$0 \leqslant \phi^\nu \leqslant 1, \qquad \phi^{\rm i} + \phi^{\rm w} + \phi^{\rm b} + \phi^{\rm a} = 1. \tag{2.1}$$

The matrix *porosity*

$$\phi^{\rm p} = \phi^{\rm w} + \phi^{\rm b} + \phi^{\rm a} = 1 - \phi^{\rm i}, \tag{2.2}$$

and the volume fractions of mobile water, bound water and air per unit pore volume are obtained by dividing their mixture volume fractions by the porosity:

$$\theta^{\rm w} = \phi^{\rm w}/\phi^{\rm p}, \qquad \theta^{\rm b} = \phi^{\rm b}/\phi^{\rm p}, \qquad \theta^{\rm a} = \phi^{\rm a}/\phi^{\rm p}. \tag{2.3}$$

It is also useful to identify the links between these definitions and those of Colbeck & Anderson (1982). The total *water saturation* $S_{\rm w} = \theta^{\rm w} + \theta^{\rm b}$, the *irreducible water saturation* $S_{\rm wi} = \theta^{\rm b}$ and the *effective water saturation*

$$S_{\rm e} = \frac{S_{\rm w} - S_{\rm wi}}{1 - S_{\rm wi}} = \frac{\theta^{\rm w}}{1 - \theta^{\rm b}}. \tag{2.4}$$

The balance laws are formulated in terms of *partial* variables, which are defined per unit mixture volume and denoted by a lower case superscript. An essential feature of mixture theory is the link between the partial variables and the *intrinsic* variables which are associated with material elements of an individual constituent, and are denoted by an upper case superscript. Essentially all variables, apart from the partial and intrinsic velocity fields which are identical, are related by a linear volume fraction scaling. For example, the partial and intrinsic densities of each of the constituents are linked by

$$\rho^{\rm i} = \phi^{\rm i}\rho^{\rm I}, \qquad \rho^{\rm w} = \phi^{\rm w}\rho^{\rm W}, \qquad \rho^{\rm b} = \phi^{\rm b}\rho^{\rm W}, \qquad \rho^{\rm a} = \phi^{\rm a}\rho^{\rm A}. \tag{2.5}$$

A detailed discussion of these relations and general mixture theory is presented by Morland (1992).

The three-dimensional mixture conservation laws for a four constituent snow pack incorporating water vapour, but not distinguishing mobile and bound water, were derived by Morland *et al.* (1990). Following the reduced formulations of Gray & Morland (1994) and Gray *et al.* (1995), we focus our attention on a one-dimensional vertical snow pack in which there are no lateral gradients and the horizontal velocity components are identically zero. The coordinate z measures distance in the vertically downward sense and v^ν is the vertical velocity of constituent ν.

Mass balance for constituent ν is expressed by

$$\frac{\partial \rho^\nu}{\partial t} + \frac{\partial}{\partial z}(\rho^\nu v^\nu) = m^\nu, \tag{2.6}$$

where m^ν is the rate of mass supply per unit mixture volume to constituent ν by all the other constituents. This can be decomposed into the individual rates of mass supply, $m^{\nu\omega}$, to constituent ν from constituent ω per unit mixture volume, so that $m^\nu = \sum_\omega m^{\nu\omega}$ (summation over $\omega = \mathrm{i}, \mathrm{w}, \mathrm{b}, \mathrm{a}$). The rate of mass supply from each constituent to itself, $m^{\nu\nu}$, is by definition zero, and the rate of mass supply from constituent ν to constituent ω is equal but opposite in sign to the rate of mass supply from ω to ν, $m^{\nu\omega} = -m^{\omega\nu}$. It follows that the sum of the rate of mass supplies m^ν over all constituents ν is equal to zero, that is $\sum_\nu m^\nu = 0$. Note that $m^{a\nu} = 0$ is assumed here since the air is inert.

In the slow flow regime that dominates in wet snow packs the acceleration terms can be neglected in the linear momentum balance for each constituent ν, which then take the form

$$-\frac{\partial p^\nu}{\partial z} + \rho^\nu g + \rho \mathcal{B}^\nu = \frac{1}{2}\sum_\omega m^{\nu\omega}(v^\nu - v^\omega), \tag{2.7}$$

where g is the constant of gravitational acceleration and the bulk mixture density $\rho = \sum_\nu \rho^\nu$. The interaction drag $\mathcal{B}^\nu$ per unit mass of mixture represents the net effect of tractions across interfaces with all other constituents and its sum $\sum_\nu \mathcal{B}^\nu = 0$ by definition. The terms on the right-hand side of (2.7) represent momentum transfer between constituents due to phase change, and were called thrusts by Morland (1992) to distinguish them from the interaction drags $\mathcal{B}^\nu$ which are due to the resistance to relative motion. These contributions do not sum to zero in general $\sum_\nu \sum_\omega m^{\nu\omega}(v^\nu - v^\omega) = 2\sum_\nu m^\nu v^\nu \neq 0$, so the momentum transfers due to phase change can effect the bulk mixture response since part of the system mass is changing velocity.

The four constituents are in a state of thermal equilibrium, provided that the forcing timescale is much longer than the timescale for thermal transfers between constituents, which is assumed here. Thus, all constituents have a common temperature, T, and there is a single bulk energy balance (Morland *et al.* 1990)

$$\sum_\nu \left[\rho^\nu C_p^{\mathcal{N}} \frac{D_\nu T}{Dt} - \rho^\nu r^\nu - \frac{p^\nu}{\phi^\nu}\frac{D_\nu \phi^\nu}{Dt}\right] - \frac{\partial}{\partial z}\left(\sum_\nu \phi^\nu K^{\mathcal{N}} \frac{\partial T}{\partial z}\right) = (m^{\mathrm{iw}} + m^{\mathrm{ib}})L_{\mathrm{iw}}, \tag{2.8}$$

where for constituent ν, $C_p^{\mathcal{N}}$ is the specific heat at constant pressure ($\mathcal{N}$ is a capital ν), $K^{\mathcal{N}}$ is the thermal conductivity and r^ν is the rate of external energy supply per unit volume of mixture. The total external energy supply per unit mixture volume $I = \sum_\nu \rho^\nu r^\nu$ is regarded as an externally prescribed function. In the context of snow this term represents the energy deposited by solar radiation in the top ten centimetres of the pack. Colbeck (1989) used an inverse exponential function to characterize its decay with increasing depth. Phase change only takes place between the ice matrix and the water components, and so the latent heat released as water turns into ice, L_{iw}, is the only contribution to the energy balance. The convected derivative D_ν/Dt, defined as

$$\frac{D_\nu}{Dt} = \frac{\partial}{\partial t} + v^\nu \frac{\partial}{\partial z}, \tag{2.9}$$

is the rate of the change with time following a particle of constituent ν. All the thermal constants are summarized in table 1.

Table 1. *Constants*

constant	SI value
gravity acceleration, g	$9.81\ \mathrm{m\ s^{-2}}$
air gas constant, R^{A}	$2.8704 \times 10^3\ \mathrm{J\ kg^{-1}\ K^{-1}}$
melting point, T_{M}	273.2 K
ice density, ρ^{I}	$0.918 \times 10^3\ \mathrm{kg\ m^{-3}}$
water density, ρ^{W}	$10^3\ \mathrm{kg\ m^{-3}}$
viscosity of air, μ^{A}	$1.45 \times 10^{-5}\ \mathrm{kg\ m^{-1}\ s^{-1}}$
viscosity of water, μ^{W}	$8.91 \times 10^{-4}\ \mathrm{kg\ m^{-1}\ s^{-1}}$
specific heat ice, C_p^{I}	$2.093 \times 10^3\ \mathrm{J\ kg^{-1}\ K^{-1}}$
specific heat water, C_p^{W}	$4.192 \times 10^3\ \mathrm{J\ kg^{-1}\ K^{-1}}$
specific heat air, C_p^{A}	$1.012 \times 10^3\ \mathrm{J\ kg^{-1}\ K^{-1}}$
thermal conductivity ice, K^{I}	$2.2\ \mathrm{J\ m^{-1}\ s^{-1}\ K^{-1}}$
thermal conductivity water, K^{W}	$0.58\ \mathrm{J\ m^{-1}\ s^{-1}\ K^{-1}}$
thermal conductivity air, K^{A}	$2.24 \times 10^{-2}\ \mathrm{J\ m^{-1}\ s^{-1}\ K^{-1}}$
latent heat of melting, L_{iw}	$3.34 \times 10^5\ \mathrm{J\ kg^{-1}}$

3. Constitutive postulates

The basic mixture framework must be supplemented by constitutive postulates to obtain a closed system of equations. The number of postulates required is determined by subtracting the total number of conservation balances and algebraic relations, from the total number of independent variables. For simplicity no distinction is drawn between partial and intrinsic variables in the variable count as the relations between them are implicitly assumed from the mixture theory definitions. In the four constituent wet snow pack theory of § 2 there are a total of 22 independent fields. Namely, four densities ρ^{i}, ρ^{w}, ρ^{b}, ρ^{a}, four pressures p^{i}, p^{w}, p^{b}, p^{a}, four velocities v^{i}, v^{w}, v^{b}, v^{a}, three volume fractions ϕ^{i}, ϕ^{w}, ϕ^{b} (the fourth ϕ^{a} is given by the sum $\sum_\nu \phi^\nu = 1$), three interaction drags $\mathcal{B}^{\mathrm{w}}$, $\mathcal{B}^{\mathrm{b}}$, $\mathcal{B}^{\mathrm{a}}$, (the fourth is given by the sum $\sum_\nu \mathcal{B}^\nu = 0$), three rates of mass supply m^{iw}, m^{ib}, m^{wb}, and one temperature T. The conservation relations yield four mass balances (2.6), four momentum balances (2.7), and one bulk energy balance (2.8), a total of 9 equations, so 13 constitutive postulates are required to close the problem. These are now catalogued and discussed below.

The ice and water are assumed to have constant intrinsic densities and the air satisfies an ideal gas law (postulates 1, 2, 3 and 4):

$$\rho^{\mathrm{I}} = 918, \quad \rho^{\mathrm{W}} = 1000, \quad \rho^B = \rho^{\mathrm{W}}, \quad p^{\mathrm{A}} = \rho^{\mathrm{A}} R^{\mathrm{A}} T, \tag{3.1}$$

where all the densities are measured in $\mathrm{kg\ m^{-3}}$ and the air gas constant $R^{\mathrm{A}} = 2.87 \times 10^2\ \mathrm{J\ kg^{-1}\ K^{-1}}$ (Gill 1982).

The amount of water trapped in the pore space is, in general, a function of the porosity, grain size and wetting history. History dependence stems from the fact that there is a greater probability that water arrived at a location where it could become trapped, if at some point the water occupied a greater proportion of the pore space. It is, however, common to assume that the irreducible water saturation S_{wi} is a

constant and here we follow Colbeck (1974) (postulate 5)

$$S_{\mathrm{wi}} = \theta^{\mathrm{b}} = 0.07, \tag{3.2}$$

although different values have been used, for example, Ambach *et al.* (1981) choose a value of 0.03 and Bengtsson (1982) used 0.05. This of course implies that the saturation per unit mixture volume, $\phi^{\mathrm{b}} = \phi^{\mathrm{p}} S_{\mathrm{wi}}$, increases linearly with porosity. Postulate (3.2) is probably far too restrictive and further work (which is beyond the scope of this paper) is needed to build in the dependence on grain size and wetting history.

Water released into the snow pack either by internal phase change or by surface drainage, subsequently percolates down through the pack under the action of gravity. The water does not occupy all the pore space except when there is some blocking of the pores and, in general, the flow is unsaturated with the rest of the space filled by air. The flow of two immiscible fluids (air and water in this case) is still described by Darcy's law (Scheidegger 1960; Bear 1972) which is delivered by the interaction drags (postulates 6 and 7)

$$\rho \mathcal{B}^{\mathrm{w}} = p^{\mathrm{W}} \frac{\partial \phi^{\mathrm{w}}}{\partial z} - \frac{\mu^{\mathrm{w}}}{k^{\mathrm{w}}} (\phi^{\mathrm{w}})^2 (v^{\mathrm{w}} - v^{\mathrm{i}}), \tag{3.3}$$

$$\rho \mathcal{B}^{\mathrm{a}} = p^{\mathrm{A}} \frac{\partial \phi^{\mathrm{a}}}{\partial z} - \frac{\mu^{\mathrm{a}}}{k^{\mathrm{a}}} (\phi^{\mathrm{a}})^2 (v^{\mathrm{a}} - v^{\mathrm{i}}), \tag{3.4}$$

(Morland 1978) where $\mu^{\mathrm{W}} = 8.91 \times 10^{-4}\ \mathrm{kg\ m^{-1}\ s^{-1}}$ is the viscosity of water and $\mu^{\mathrm{A}} = 1.45 \times 10^{-5}\ \mathrm{kg\ m^{-1}\ s^{-1}}$ is the viscosity of air (Batchelor 1967; Weast 1988). However, the concept of matrix permeability must be re-interpreted. The permeabilities k^{w}, k^{a} are not equal to the intrinsic matrix permeability k (for which Kuriowa (1968) proposes a dependence on matrix porosity $k = a \exp(b\phi^{\mathrm{p}})$ with $a = 0.625 \times 10^{-13}\ \mathrm{m^2}$, $b = 15.9$), but are the *effective* permeabilities of the matrix to water and air, respectively. The *relative* permeabilities to each phase are defined by the ratios

$$k^{\mathrm{rw}} = k^{\mathrm{w}}/k, \qquad k^{\mathrm{ra}} = k^{\mathrm{a}}/k, \tag{3.5}$$

where $0 \leqslant k^{\mathrm{rw}}, k^{\mathrm{ra}} \leqslant 1$. The relative permeability to one phase is a function only of saturation of that phase, an assumption that numerous experiments (Scheidegger 1960) seem to verify. We shall assume that

$$k^{\mathrm{rw}} = k^{\mathrm{rw}}(S_{\mathrm{e}}), \tag{3.6}$$

where the saturation has been interpreted as the volume fraction per unit effective pore space $\phi^{\mathrm{e}} = \phi^{\mathrm{w}} + \phi^{\mathrm{a}}$; that is, the actual pore space minus the volume fraction occupied by the bound water. As the effective water saturation approaches unity, $S_{\mathrm{e}} \to 1$, the effective permeability tends to the permeability of a single fluid, $k^{\mathrm{w}} \to k$ from below. A power law relation (Morel-Seytoux 1969),

$$k^{\mathrm{rw}} = (S_{\mathrm{e}})^n, \tag{3.7}$$

where n is a real, was adopted by Colbeck (1971, 1972) with $n = 2$ to derive some elementary solutions. Colbeck & Davidson (1973) used drainage tests to deduce $n \simeq 3.3$ and Colbeck (1974) used $n = 3$ to simplify his mathematical analysis.

A discontinuity in pressure exists across the interface separating the air and water, and its magnitude is dependent on the interface curvature. The difference in pressure is called the *capillary pressure*

$$p^{\mathrm{C}} = p^{\mathrm{A}} - p^{\mathrm{W}} > 0 \tag{3.8}$$

PHILOSOPHICAL TRANSACTIONS OF THE ROYAL SOCIETY A MATHEMATICAL, PHYSICAL & ENGINEERING SCIENCES

as the water is *hydroscopic*. The curvature of the interface is dependent on the effective water saturation and, therefore, the capillary pressure is also dependent on S_e (postulate 8),

$$p^C = p^C(S_e), \tag{3.9}$$

though the precise functional relation for each material must be determined experimentally. Colbeck (1974) deduced a capillary pressure/liquid saturation relation for small grained snow and kerosene at $-10\,^\circ$C. Although there were only two data points in the significant region of normal mobile water saturation (0–10%) Colbeck suggested a functional form

$$p^C = 43/S_e + 380 \text{ Pa}. \tag{3.10}$$

This has the unfortunate property that the capillary pressure becomes unbounded in the limit as the effective water saturation tends to zero. A physically realistic model can not support infinite pressures as these would produce infinite forces in the momentum balance and drive unbounded flows. Colbeck's model only works because the Darcy drag (3.3) with the power law relative permeability (3.7) introduces another singularity $1/S_e^n$ which fortuitously cancels out the unbounded pressure gradients (provided $n \geqslant 2$). In § 6 we demonstrate how these singularities can be removed by using different relative permeability and capillary pressure relations to those of Colbeck.

Wet snow packs are characterized by the co-existence of ice, liquid water and water vapour which occurs when the temperature lies at the triple-point. In general, this is dependent on both the capillary pressure p^C and grain size (Colbeck 1973, 1975, 1982, 1987). Small fluctuations in temperature arise from these curvature effects which result in a recrystallization (metamorphism) of the snow pack. Morris & Godfrey (1978) used a relation of the form (postulate 9)

$$T = T_M + 8 \times 10^{-7} p^C - 5 \times 10^{-7} d^{-1}, \tag{3.11}$$

where $T_M = 273.1$ K (Hobbs 1974) is a fixed melt temperature, d is the diameter of a snow grain, and all the variables are measured in SI units. Note, that if Colbeck's (1974) capillary pressure relation (3.10) is substituted into (3.11), then the temperature also becomes unbounded in the limit as the saturation tends to zero. This is also physically unacceptable and presents us with another compelling reason to construct a properly posed theory in which all terms remain bounded. If we suppose that absolute tension in the water is not permitted then the upper bound for the capillary pressure might be the atmospheric pressure, $p^A \simeq 10^5$ Pa, and fluctuations in temperature would be of order 0.1 K. Maximum capillary pressures are probably closer to 2×10^3 Pa in magnitude, which implies temperature fluctuations of order 10^{-3} K. This paper does not include a model for the evolution of the grain size d due to metamorphism, although this will be a natural extension when the singularities present in the existing theory have been removed. Here the grain size is assumed to be a constant throughout the entire pack, and it follows that the last term on the right-hand side of (3.11) has a uniform constant value.

The rate of mass supply m^i from the ice matrix to the water, must be decomposed into the contributions to both the mobile and immobile water phases. The natural mixture partitioning is adopted here, in which the amount that is transferred to each phase is weighted by the relative proportions of bound and mobile water (postulate

10):

$$m^{\mathrm{iw}} = \eta m^{\mathrm{i}}, \quad m^{\mathrm{ib}} = (1-\eta)m^{\mathrm{i}}, \tag{3.12}$$

where

$$\eta = \frac{\phi^{\mathrm{w}}}{\phi^{\mathrm{w}} + \phi^{\mathrm{b}}} = \frac{\theta^{\mathrm{w}}}{\theta^{\mathrm{w}} + \theta^{\mathrm{b}}}. \tag{3.13}$$

Other models for η are possible. For instance one could assume that all the melt water is transferred into bound water ($\eta = 0$), or into mobile water ($\eta = 1$), and then the rate of mass supply between the bound and mobile water m^{wb} maintains the constant irreducible water saturation.

The bound water is trapped in the necks of the ice grain boundaries and is assumed to have the same velocity as the ice matrix (postulate 11)

$$v^{\mathrm{b}} = v^{\mathrm{i}}, \tag{3.14}$$

the force necessary to do this is supplied by the interaction drag $\mathcal{B}^{\mathrm{b}}$. The bound water pressure has received very little or no attention in previous studies, since their equations uncouple p^{b} from the saturation equation. Here we propose that the bound water pressure is constant (postulate 12)

$$p^{B} = p^{\mathrm{W}}|_{S_{\mathrm{e}}=0}, \tag{3.15}$$

so that in general a pressure jump exists between mobile and bound water except in the limit as $S_{\mathrm{e}} \to 0$. This is intended to reflect the fact that there is very little mutual interaction between the two phases at low saturation.

To complete the catalogue of constitutive properties a law is required for the ice matrix pressure p^{i}, which controls the compaction of the snow pack. This is notoriously difficult to pin down. The mechanical properties of all forms of snow were reviewed by Mellor (1975). He concluded that they exhibited such bewildering complexities that it was necessary to adopt greatly simplified descriptions, concentrating on the characteristics that dominate in a particular problem. To maintain sufficient generality, therefore, we do not explicitly prescribe a precise functional form of the constitutive relation (appropriate for a particular wet snow pack) in this paper. We merely require that one exists (postulate 13).

4. Model equations

The conservation balances in conjunction with the thirteen constitutive postulates define a closed system of equations for 22 independent variables. Using (3.1), (3.12) and (3.14) the four mass balances (2.6) are

$$\rho^{\mathrm{I}}\left\{\frac{\partial \phi^{\mathrm{i}}}{\partial t} + \frac{\partial}{\partial z}(\phi^{\mathrm{i}} v^{\mathrm{i}})\right\} = m^{\mathrm{i}}, \tag{4.1}$$

$$\rho^{\mathrm{W}}\left\{\frac{\partial \phi^{\mathrm{w}}}{\partial t} + \frac{\partial}{\partial z}(\phi^{\mathrm{w}} v^{\mathrm{w}})\right\} = m^{\mathrm{wb}} - \eta m^{\mathrm{i}} \tag{4.2}$$

$$\rho^{\mathrm{W}}\left\{\frac{\partial \phi^{\mathrm{b}}}{\partial t} + \frac{\partial}{\partial z}(\phi^{\mathrm{b}} v^{\mathrm{i}})\right\} = -m^{\mathrm{wb}} - (1-\eta)m^{\mathrm{i}} \tag{4.3}$$

$$\frac{\partial}{\partial t}(\phi^{\mathrm{a}}\rho^{\mathrm{A}}) + \frac{\partial}{\partial z}(\phi^{\mathrm{a}}\rho^{\mathrm{A}} v^{\mathrm{a}}) = 0, \tag{4.4}$$

PHILOSOPHICAL TRANSACTIONS OF THE ROYAL SOCIETY A MATHEMATICAL, PHYSICAL & ENGINEERING SCIENCES

for the ice, mobile water, bound water and air, respectively. Substituting the mobile water and air interaction drags (3.3), (3.4) into their respective momentum balances (2.7) we obtain

$$-\frac{\partial p^{\mathrm{W}}}{\partial z}+\rho^{\mathrm{W}}g-\frac{\mu^{\mathrm{W}}}{k^{\mathrm{w}}}\phi^{\mathrm{w}}(v^{\mathrm{w}}-v^{\mathrm{i}})=\frac{1}{2\phi^{\mathrm{w}}}(\eta m^{\mathrm{i}}-m^{\mathrm{wb}})(v^{\mathrm{i}}-v^{\mathrm{w}}), \tag{4.5}$$

$$-\frac{\partial p^{\mathrm{A}}}{\partial z}+\rho^{\mathrm{A}}g-\frac{\mu^{\mathrm{A}}}{k^{\mathrm{a}}}\phi^{\mathrm{a}}(v^{\mathrm{a}}-v^{\mathrm{i}})=0, \tag{4.6}$$

where the partitioning relation (3.12) and common velocity assumption (3.14) have been used to simplify the interaction thrust terms. Alternately summing and differencing the ice and bound water momentum balances and using the summation relation $\sum_\nu \mathcal{B}^\nu=0$ implies

$$-\frac{\partial}{\partial z}(p^{\mathrm{i}}\pm p^{\mathrm{b}})+(\rho^{\mathrm{i}}\pm\rho^{\mathrm{b}})g-\rho(\mathcal{B}^{\mathrm{w}}+\mathcal{B}^{\mathrm{a}})-\tfrac{1}{2}(\eta m^{\mathrm{i}}\mp m^{\mathrm{wb}})(v^{\mathrm{i}}-v^{\mathrm{w}})=\begin{cases}0\\ 2\rho\mathcal{B}^{\mathrm{b}}\end{cases} \tag{4.7}$$

respectively. The sum relation is an equation for the compaction of the ice matrix, while the difference relation determines the interaction drag $\mathcal{B}^{\mathrm{b}}$ necessary to maintain the common velocity (3.14). Finally, substituting the triple-point temperature (3.11) into the energy balance (2.8) determines the rate of mass supply to the ice from the water, m^{i},

$$\sum_\nu\left[\alpha\rho^\nu C_p^{\mathcal{N}}\frac{D_\nu p^{\mathrm{C}}}{Dt}-\alpha\frac{\partial}{\partial z}\left(\phi^\nu K^{\mathcal{N}}\frac{\partial p^{\mathrm{C}}}{\partial z}\right)-\frac{p^\nu}{\phi^\nu}\frac{D_\nu\phi^\nu}{Dt}\right]=I+m^{\mathrm{i}}L_{\mathrm{iw}}, \tag{4.8}$$

where $\alpha=8\times10^{-7}\,\mathrm{K\,Pa^{-1}}$ is the constant of proportionality in the triple-point temperature relation (3.11). The dominant balance in this equation lies between the external energy supply, I, from solar radiation and the latent heat term $m^{\mathrm{i}}L_{\mathrm{iw}}$. The solar radiation term has magnitude $I\sim400\,\mathrm{W\,m^{-3}}$, which implies that the rate of mass supply $m^{\mathrm{i}}\sim10^{-3}\,\mathrm{kg\,m^{-3}\,s^{-1}}$ in the near surface layers. Deeper inside the pack where solar radiation has been attenuated the variations in temperature are controlled by the curvature effects, and the amount of phase change is considerably reduced. If capillary pressures $p^{\mathrm{C}}\sim10^5$ Pa change by their own order of magnitude on diurnal time-scales $t_d=2\times10^4$ s, then the local heating term $|\alpha\rho^{\mathrm{I}}C_p^{\mathrm{I}}\partial p^{\mathrm{C}}/\partial t|\sim10\,\mathrm{W\,m^{-3}}$ and the rate of mass supply $m^{\mathrm{i}}\sim10^{-4}\,\mathrm{kg\,m^{-3}\,s^{-1}}$, which is probably still somewhat large. A more realistic capillary pressure magnitude $p^{\mathrm{C}}\sim2\times10^3$ Pa, however, implies local heating $|\alpha\rho^{\mathrm{I}}C_p^{\mathrm{I}}\partial p^{\mathrm{C}}/\partial t|\sim10^{-1}\,\mathrm{W\,m^{-3}}$ and mass supplies $m^{\mathrm{i}}\sim10^{-6}\,\mathrm{kg\,m^{-3}\,s^{-1}}$, which are 10^3 smaller than in the near surface layers. Note, that for these estimates of the local heating term Morland *et al.*'s (1990) reduced energy balance (adopted here) can still be applied without introducing interaction drag working or pressure rate terms which are at most $10^{-5}\,\mathrm{W\,m^{-3}}$.

With the above estimates the maximum rate of mass supply $m^{\mathrm{i}}\sim10^{-3}\,\mathrm{kg\,m^{-3}\,s^{-1}}$ and the thrust terms $|m^{\mathrm{i}}v^{\mathrm{w}}|\sim10^{-7}\,\mathrm{kg\,m^{-2}\,s^{-2}}$ for a maximum water velocity magnitude $v^{\mathrm{w}}\sim10^{-4}\,\mathrm{m\,s^{-1}}$, which is negligible compared to gravitational forces $\rho^{\mathrm{W}}g\sim10^4\,\mathrm{kg\,m^{-2}\,s^{-2}}$. The interaction thrust terms in equations (4.5) and (4.7) can therefore be neglected. Note, that if the capillary pressure relation (3.10) is substituted into (4.8) then unbounded rates of mass supply m^{i} and unbounded interaction thrusts are produced in the limit as $S_{\mathrm{e}}\to0$ underlining once again that finite capillary pressures are required in a properly posed theory.

It is of interest to make a few basic deductions regarding the rates of mass supply m^{i} and m^{wb} in light of the rather simple irreducible water saturation postulate (3.2) and the rate of mass supply partitioning (3.12). Multiplying the ice mass balance (4.1) by the constant $\rho^{\mathrm{W}} S_{\mathrm{wi}}/\rho^{\mathrm{I}}$ and summing with the bound water mass balance (4.3), using the identity $\phi^{\mathrm{i}} + \phi^{\mathrm{p}} = 1$, implies

$$\rho^{\mathrm{W}} S_{\mathrm{wi}} \frac{\partial v^{\mathrm{i}}}{\partial z} = -\left[1 - \eta - \rho^{\mathrm{W}} \frac{S_{\mathrm{wi}}}{\rho^{\mathrm{I}}}\right] m^{\mathrm{i}} - m^{\mathrm{wb}}, \tag{4.9}$$

which determines the mass transfer m^{wb} between bound and mobile water as a function of the ice matrix compaction and phase change m^{i}. In the special case when there is no compaction ($\partial v^{\mathrm{i}}/\partial z = 0$) the direction for the mass transfer m^{wb} is dependent on the sign of the square bracketed term in (4.9). If $\theta^{\mathrm{w}} \leqslant \rho^{\mathrm{I}}/\rho^{\mathrm{W}} - S_{\mathrm{wi}} \simeq 0.85$ then $[.] \geqslant 0$ and bound water is supplied to the mobile water ($m^{\mathrm{wb}} > 0$) during melting ($m^{\mathrm{i}} < 0$) and mobile water is supplied to the bound water ($m^{\mathrm{wb}} < 0$) during freezing ($m^{\mathrm{i}} > 0$). At very high saturation $\theta > \rho^{\mathrm{I}}/\rho^{\mathrm{W}} - S_{\mathrm{wi}}$ the bracket $[.] < 0$ and the direction of the mass supplies m^{wb} is reversed. Similarly, in the special case when there is no phase change ($m^{\mathrm{i}} = 0$) compaction ($\partial v^{\mathrm{i}}/\partial z < 0$) will release bound water into the mobile phase ($m^{\mathrm{wb}} > 0$) and if extension is possible mobile water will be supplied to the bound water ($m^{\mathrm{wb}} < 0$). These simple deductions fail if more general irreducible water saturation dependencies on porosity, grain size and wetting history are considered. Postulates (3.2) and (3.12) clearly have an important effect on determining the amount of mobile water available to flow through the ice matrix.

It is also possible to obtain an equation for the effective saturation of a more general form than has hitherto been derived. Taking the difference of the water and air momentum balances (4.5) and (4.6), with the further observations that $\rho^{\mathrm{A}} \ll \rho^{\mathrm{W}}$ and $\mu^{\mathrm{A}} \ll \mu^{\mathrm{W}}$, the water flux

$$u^{\mathrm{w}} = \phi^{\mathrm{w}} v^{\mathrm{w}} = \phi^{\mathrm{w}} v^{\mathrm{i}} + \frac{k^{\mathrm{rw}}}{(\mu^{\mathrm{W}}/k)} \left(\frac{\partial p^{\mathrm{C}}}{\partial z} + \rho^{\mathrm{W}} g\right), \tag{4.10}$$

and substituting this into the water mass balance (4.2), we obtain

$$\frac{\partial}{\partial t}(\phi^{\mathrm{e}} S_{\mathrm{e}}) + \frac{\rho^{\mathrm{W}} g}{\mu^{\mathrm{W}}/k} \frac{\partial}{\partial z}(k^{\mathrm{rw}}) + \frac{1}{\mu^{\mathrm{W}}/k} \frac{\partial}{\partial z}\left(k^{\mathrm{rw}} \frac{\partial p^{\mathrm{C}}}{\partial z}\right) + \frac{\partial}{\partial z}(\phi^{\mathrm{e}} S_{\mathrm{e}} v^{\mathrm{i}}) = m^{\mathrm{wb}} - \eta m^{\mathrm{i}}, \tag{4.11}$$

where the effective porosity $\phi^{\mathrm{e}} = \phi^{\mathrm{p}}(1 - S_{\mathrm{wi}})$. The first three terms are those conventionally used in melt water percolation problems (in a slightly more general form). The fourth term arises from the deformation of the ice matrix. While the terms on the right-hand side are the rates of mass supply from the bound water and the ice matrix, which are at least as important as the conventional terms in the near surface layers.

5. Simplified model

To investigate the percolation problem at greater length two further restrictions are imposed in order to uncouple the effective saturation from the deformation of the pack and phase change. These restrictions are assumed in Colbeck's (1974) theory, but never explicitly stated, and we stress that they do not follow from the order of magnitude estimates in § 4. This simplified model therefore does not represent a

reduced theory in which small terms have been neglected in a rational and consistent manner.

The restrictions are that the pack is pre-compacted, so that the ice matrix is stationary, and that there is no phase change

$$v^{\mathrm{i}} \equiv 0, \quad m^{\mathrm{i}} \equiv 0. \tag{5.1}$$

These may well be appropriate leading order approximations in the interior of a ripe snow pack with negligible deformation, but will almost certainly fail during rapid deformations of the ice matrix and when significant phase change is taking place. For instance at the surface of the pack and possibly close to sharp fronts where the relevant time-scale is shorter than the diurnal time-scale assumed in the order of magnitude estimates in § 4.

Given these two restrictions it follows from the ice mass balance (4.1) that the ice matrix and effective porosity are independent of time, and from relation (4.9) that the rate of mass supply from bound water to the mobile water is zero

$$\phi^{\mathrm{p}} = \phi^{\mathrm{p}}(z), \quad \phi^{\mathrm{e}} = \phi^{\mathrm{e}}(z), \quad m^{\mathrm{wb}} = 0 \tag{5.2}$$

(recall $\phi^{\mathrm{e}} = \phi^{\mathrm{p}}(1 - S_{\mathrm{wi}})$). The effective saturation equation (4.11) then reduces to the conventional form

$$\phi^{\mathrm{e}} \frac{\partial S_{\mathrm{e}}}{\partial t} + \frac{\rho^{\mathrm{W}} g}{\mu^{\mathrm{W}}/k} \frac{\partial}{\partial z}(k^{\mathrm{rw}}) = -\frac{1}{\mu^{\mathrm{W}}/k} \frac{\partial}{\partial z}\left(D \frac{\partial S_{\mathrm{e}}}{\partial z} \right), \tag{5.3}$$

(by construction) where the diffusion coefficient $D = D(S_{\mathrm{e}})$ equals

$$D = k^{\mathrm{rw}} \frac{\mathrm{d}p^{\mathrm{C}}}{\mathrm{d}S_{\mathrm{e}}}. \tag{5.4}$$

The restrictions (5.1) achieve great simplification while preserving the essential mathematical structure of interest to us. These simplified equations are therefore adopted throughout the remainder of this paper in order to demonstrate how the singularities introduced by the capillary pressure (3.10) and the relative permeability (3.7) can be removed. The model functions presented in § 7 *d* have the desired properties for a well-posed theory and can be applied in the full mixture equations (4.1)–(4.8) to solve more general problems with internal phase change and compaction.

We shall consider two forcing scenarios in which the volume flux of mobile water, $u^{\mathrm{w}} = \phi^{\mathrm{w}} v^{\mathrm{w}}$, entering the snow pack takes two extreme values. For the large estimate the magnitude of the mobile water volume flux, u_{w}^{*}, the maximum volume flux used by Colbeck (1974) is adopted,

$$u_{\mathrm{w}}^{*} = 1.2 \times 10^{-6} \text{ or } 1.2 \times 10^{-7} \ \mathrm{m\,s^{-1}}, \tag{5.5}$$

and the estimate for a smaller magnitude is then chosen to be one tenth of this value. If a balance exists between the viscous Darcy drags and the gravitational force in (4.5), then

$$k^{\mathrm{rw}} \sim \gamma u_{\mathrm{w}}^{*}, \tag{5.6}$$

estimates the relative permeability, where $\gamma = (\mu^{\mathrm{W}}/k)/(\rho^{\mathrm{W}} g) \simeq 3.33 \times 10^{2} \ \mathrm{s\,m^{-1}}$ for a matrix permeability $k = 3 \times 10^{-10} \ \mathrm{m^{2}}$ (Colbeck 1974). For the power law dependence (3.7) the relative permeability $k^{\mathrm{rw}} \sim (S^{*})^{n}$. It follows by substituting this into (5.6) that the mobile water saturation and velocity magnitudes are

$$S^{*} = \gamma^{1/n} {u_{\mathrm{w}}^{*}}^{1/n}, \qquad v_{\mathrm{w}}^{*} = \gamma^{-1/n} {u_{\mathrm{w}}^{*}}^{1-1/n} / \phi_{\mathrm{e}}^{*}, \tag{5.7}$$

for an effective porosity of magnitude ϕ_e^*. In this study ϕ_e^* is assumed equal to 0.5 throughout. This suggests a scaling of the form,

$$S_e = S^* \tilde{S}, \quad v^w = v_w^* \tilde{v}^w, \quad \phi^e = \phi_e^* \tilde{\phi}^e, \tag{5.8}$$

where the superposed tilde denotes a non-dimensional variable, which is order unity or less, and the stars indicate the magnitude of that variable. For exponent $n = 2$ (Colbeck 1972) the mobile water saturation $S^* = 0.02$ or 0.006, and the velocity $v_w^* = 1.2 \times 10^{-4}$ or 3.8×10^{-5} m s^{-1} (10.3 m d^{-1} or 3.2 m d^{-1}) for the two u_w^* extremes in (5.5), respectively. Increasing the exponent n to 3 (Colbeck 1974) results in higher saturation $S^* = 0.074$ or 0.034 and correspondingly lower velocities $v_w^* = 3.2 \times 10^{-5}$ or 7×10^{-6} m s^{-1} (2.7 m d^{-1} or 0.6 m d^{-1}).

Solar radiation is the dominant generation mechanism for the melt water entering the pack, and so order unity variations in the surface saturation take place on the diurnal timescale $t^d = 2 \times 10^4$ s. This has an associated length scale $z^d = v_w^* t^d$, and implies length scales of 2.4 m or 76 cm ($n = 2$) and 64 or 14 cm ($n = 3$) for the two water fluxes in (5.5). These are the natural time and length scalings that arise after neglecting the right-hand side of (5.3), when the equation has a hyperbolic structure which supports shock waves (Colbeck 1972). Here we retain the capillary pressure term and (5.3) is parabolic. This prevents the formation of shocks but does allow very steep gradients to develop near a front, where the associated length and timescales are typically much shorter. To determine the appropriate magnitudes t^*, z^* for the shock front scalings

$$t = t^* \tilde{t}, \qquad z = z^* \tilde{z}, \tag{5.9}$$

we must consider specific forms of the capillary pressure and relative permeability relations, (3.6) and (3.9). The diffusion coefficient $D(S_e)$ in (5.4) is particularly important as it identifies classes of solutions with the same mathematical behaviour. In § 6 we investigate a series of such classes.

Note, that if (5.3) is scaled to give each term equal status (a balance which exists at the front) then the frontal time t_f and length z_f scales satisfy the constraint that the two non-dimensional parameters, which proceed the nonlinear advection and diffusion terms, are equal to unity. That is,

$$\frac{\gamma S^*}{k_{rw}^*} \frac{z_f}{t_f} = 1, \qquad \frac{D^*}{(\mu^w/k)} \frac{t_f}{(z_f)^2} = 1, \tag{5.10}$$

where D^* is a magnitude for the diffusion $D(S_e)$ and k_{rw}^* is a magnitude for the relative permeability $k^{rw}(S_e)$ at a given saturation S^*. When (5.3) is scaled on a general time-scale t^* and length-scale z^*, the nonlinear advection term has equal status to the time derivative and the non-dimensional parameters are

$$\frac{\gamma S^*}{k_{rw}^*} \frac{z^*}{t^*} = 1, \qquad \frac{D^*}{(\mu^w/k)} \frac{t_d}{(z^*)^2} = \mathrm{C} \tag{5.11}$$

where C is a constant. Using (5.10) and $(5.11)_1$ this constant can be expressed in terms of the ratio of the length scales. Hence, the non-dimensional saturation equation (5.3) can be expressed in the form

$$\tilde{\phi}^e \frac{\partial \tilde{S}}{\partial \tilde{t}} + \frac{\partial}{\partial \tilde{z}}(\tilde{k}^{rw}) = -\left(\frac{z_f}{z^*}\right) \frac{\partial}{\partial \tilde{z}} \left(\tilde{D} \frac{\partial \tilde{S}}{\partial \tilde{z}} \right), \tag{5.12}$$

where $\tilde{D}$ and $\tilde{k}^{rw}$ are non-dimensional. It follows that if saturations change by their

own order of magnitude on a length z^* which is much larger than the frontal length scale z_f then the term on the right-hand side is small. This situation occurs in the expansion part of the wave, where variations occur on diurnal time and length scales (as is demonstrated by the illustrations in § 8).

6. Travelling wave solutions

(a) Class 1

The first class of problems is motivated by applying the capillary pressure relation (3.10) postulated by Colbeck (1974) in conjunction with the permeability (3.7) with exponent $n = 2$ adopted by Colbeck (1972). In this configuration the diffusion coefficient, defined in (5.4), $D = \text{const}$. That is, the capillary pressure gradient with respect to the effective saturation cancels with the relative permeability leaving a constant diffusion coefficient for all values of the saturation. Since the functional relation (3.9) for the capillary pressure is essentially unknown, we construct a class of solutions valid for real $n \geqslant 2$ where the gradient of the capillary pressure with respect to S_e is the reciprocal of the relative permeability power law (3.7). Consider then

$$k^{rw} = S_e^n, \qquad p^C = a_n/S_e^{n-1} + b_n, \qquad n \geqslant 2, \tag{6.1}$$

where by construction (5.3) becomes

$$\phi^e \frac{\partial S_e}{\partial t} + \frac{1}{\gamma}\frac{\partial}{\partial z}(S_e^n) = \frac{a_n(n-1)}{\mu^w/k}\frac{\partial^2 S_e}{\partial z^2}, \tag{6.2}$$

which has a diffusive structure. Time and length scales can be deduced by giving each term equal status and using (5.7) to substitute for the magnitude of the saturation:

$$\left.\begin{aligned} t^* &= \phi_e^* \gamma z^* (S^*)^{1-n} = \phi_e^* \lambda_n \gamma^{2/n} (u_w^*)^{2/n-2}, \\ z^* &= \lambda_n \gamma (S^*)^{1-n}, = \lambda_n \gamma^{1/n} (u_w^*)^{1/n-1}. \end{aligned}\right\} \tag{6.3}$$

where $\lambda_n = a_n(n-1)/(\mu^W/k)$. Now for $n = 2$ (Colbeck 1972) the capillary pressure relation (6.1) is identical to (3.10) (Colbeck 1974), so $a_2 = 43\ \text{N m}^{-2}$ and the appropriate time and length scales are of order $t^* = 2\times10^3$ s, $z^* = 24$ cm and $t^* = 2\times10^4$ s, $z^* = 76$ cm for the two water flux magnitudes in (5.5). At low saturation these are the same as those for diurnal forcing. However, for the higher flux the frontal length scale (24 cm) is ten times shorter than the diurnal length (2.4 m) and sharp fronts are expected to develop. A numerical algorithm to solve (6.2) at high saturation must, therefore, have a grid scale which is ten times finer than that suggested by the diurnal forcing alone in order to resolve the smallest length scale in the problem.

The non-dimensional saturation equation, obtained by substituting the scalings (5.8) and (6.3) into (6.2), is a generalization of Burgers equation (e.g. Acheson 1990), namely

$$\tilde{\phi}^e \frac{\partial \tilde{S}}{\partial \tilde{t}} + \frac{\partial}{\partial \tilde{z}}(\tilde{S}^n) = \frac{\partial^2 \tilde{S}}{\partial \tilde{z}^2}. \tag{6.4}$$

Analytic travelling wave solutions for constant far field conditions and uniform effective porosity $\tilde{\phi}^e = 1$ can be constructed for this class of problems. They are of interest for two reasons. Firstly, the behaviour near the front in a fully developed motion is similar to the travelling wave solution, because on the frontal timescale the far field conditions at the snow surface are approximately constant. Therefore,

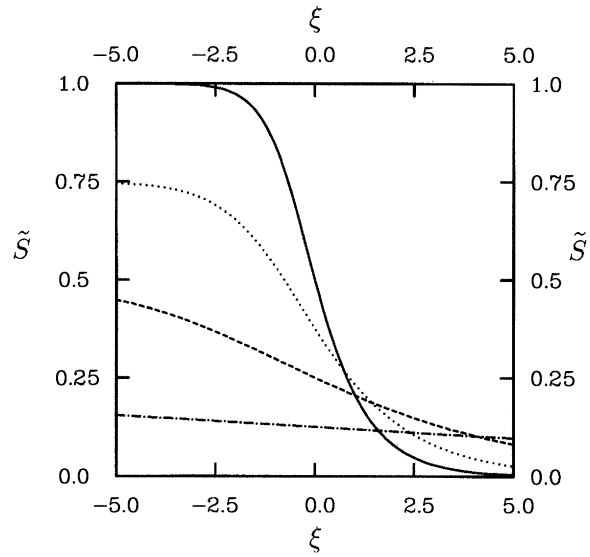

Figure 1. The class 1 travelling wave solution is illustrated for four different values of the far field saturation and exponent $n = 3$. The solid line corresponds to $S_1 = 1.0$, the dotted line to $S_1 = 0.75$, the dashed line to $S_1 = 0.5$ and the dot/dash line to $S_1 = 0.25$. Note that the solution is continuous over the whole domain, which is not physically realistic.

the shape of the front, where a balance exists between the tendency for the front to shock and diffuse, can be investigated for different far field saturations. Secondly, they provide useful special cases for testing numerical algorithms that can solve more general problems.

We seek a travelling wave solution (Acheson 1990) of the form

$$\tilde{S} = f(\xi), \qquad \xi = \tilde{z} - v\tilde{t}, \tag{6.5}$$

such that $f \to S_1$ as $\xi \to -\infty$ and $f \to 0$ as $\xi \to +\infty$. Substituting (6.5) into (6.4), integrating with respect to ξ and applying the boundary conditions, determines the front speed

$$v = S_1^{n-1}. \tag{6.6}$$

Integrating again with respect to ξ and choosing the ξ origin such that $f(0) = \frac{1}{2}S_1$ gives

$$f = S_1(1 + (2^{n-1} - 1)\exp\{\xi(n-1)S_1^{n-1}\})^{-(1/(n-1))}, \quad n \geqslant 2. \tag{6.7}$$

This solution is illustrated in figure 1 for far field saturations $S_1 = 0.25$, 0.5, 0.75 and 1.0 with exponent $n = 3$. As the far field saturation is decreased the length scales associated with order unity changes becomes much longer, which is also suggested by the scaling (6.3). Note that the solution is continuous for all ξ so that the snow surface conditions instantaneously effect the whole of the snow pack, which is physically not realistic. In figure 2 the solution is plotted with exponents $n = 2$, 3 and 4 for saturation $S_1 = 1.0$, and demonstrates that increasing the exponent n steepens the front.

(*b*) *Class 2*

The second class of solutions is motivated by the capillary pressure (3.10) proposed by Colbeck (1974) in conjunction with the relative permeability (3.7) with exponent

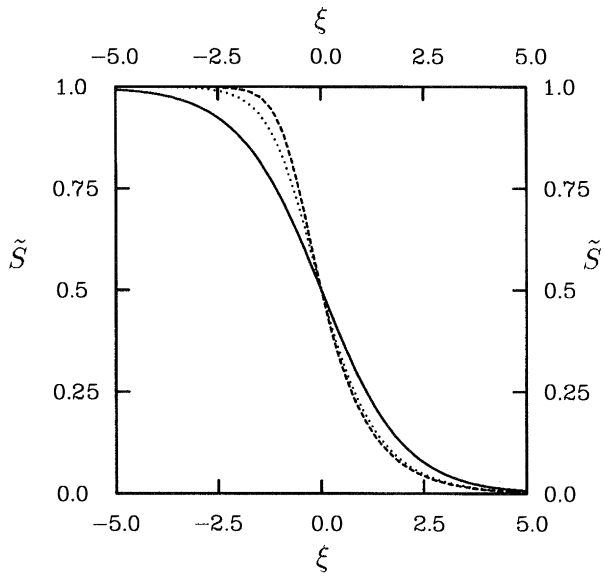

Figure 2. The class 1 travelling wave solution is illustrated for three different values of the exponent n and far field saturation $S_1 = 1.0$. The solid line corresponds to $n = 2$, the dotted line to $n = 3$ and the dashed line to $n = 4$. Increasing the exponent n steepens the front.

$n = 3$ determined by Colbeck & Davidson (1973). In this case the diffusion coefficient $D = S_e$. Again, since p^C is essentially unknown, a general class of solutions is constructed which has the property that $D = S_e$, i.e. that the capillary pressure gradient with respect to S_e multiplied by the relative permeability power law equals S_e, valid for any real $n \geqslant 3$. This requires

$$k^{rw} = S_e^n, \qquad p^C = c_n/S_e^{n-2} + d_n, \qquad n \geqslant 3. \tag{6.8}$$

When $n = 3$ this corresponds exactly to the gravity flow theory including capillary pressure gradients originally proposed by Colbeck (1974). In fact part of the motivation for the class 1 model (6.1) is simply to investigate the behaviour of Colbeck's (1974) theory when the relative permeability of Colbeck's (1972) theory is used. The saturation equation (5.3) with the class 2 assumptions (6.8) becomes

$$\phi^e \frac{\partial S_e}{\partial t} + \frac{1}{\gamma}\frac{\partial}{\partial z}(S_e^n) = \frac{c_n(n-2)}{\mu^W/k}\frac{\partial}{\partial z}\left(S_e \frac{\partial S_e}{\partial z}\right). \tag{6.9}$$

Note, that the term on the right-hand side now implies a nonlinear diffusive structure. To give each term equal status in (6.9) the length and timescales are

$$\left.\begin{aligned} t^* &= \phi_e^* \gamma z^* (S^*)^{1-n}, = \phi_e^* \psi_n \gamma^{3/n} (u_w^*)^{3/n-2}, \\ z^* &= \psi_n \gamma (S^*)^{2-n}, = \psi_n \gamma^{2/n} (u_w^*)^{2/n-1}, \end{aligned}\right\} \tag{6.10}$$

where $\psi_n = c_n(n-2)/(\mu^W/k)$. Now for $n = 3$ the capillary pressure is given by equation (3.10) so $c_3 = 43\ \mathrm{N\ m^{-2}}$ and the time and length scales are $t^* = 2 \times 10^3$ s, $z^* = 6$ cm or $t^* = 2 \times 10^4$ s, $z^* = 14$ cm for the two extreme fluxes considered. Once again the lower saturation scales are the same as those implied by diurnal forcing, but for the larger saturation the scales are ten times shorter (recall $t^d = 2 \times 10^4$ s, $z^d = 64$ cm).

Applying the scalings the non-dimensional saturation equation (6.9) becomes

$$\tilde{\phi}^{\mathrm{e}}\frac{\partial \tilde{S}}{\partial \tilde{t}} + \frac{\partial}{\partial \tilde{z}}(\tilde{S}^n) = \frac{\partial}{\partial \tilde{z}}\left(\tilde{S}\frac{\partial \tilde{S}}{\partial \tilde{z}}\right). \tag{6.11}$$

A travelling wave solution can be constructed, for uniform porosity, by substituting (6.5) into (6.11). Applying the boundary conditions $f \to S_1$ as $\xi \to -\infty$ and $f \to 0$ as $\xi \to +\infty$, determines the front speed

$$v = S_1^{n-1}, \tag{6.12}$$

which is the same as (6.6), and yield an ordinary differential equation

$$-f(S_1^{n-1} - f^{n-1}) = ff', \tag{6.13}$$

for f. This allows two possibilities,

$$f = 0, \qquad -(S_1^{n-1} - f^{n-1}) = f', \tag{6.14}$$

which admit the possibility of solutions with a discontinuous derivative. Note that in this paper we pre-suppose that the irreducible water saturation, S_{wi}, is already present throughout the pack, even in regions where there is no mobile water. In real snow packs this may not necessarily be the case and mobile water may have to be supplied to make up some, or all, of the irreducible water saturation at the front. Further treatment of this aspect of the problem is beyond the scope of this paper, but it should be noted that this feature could play an important role in the dynamics of the frontal region. Choosing an origin at $\xi = 0$ we envisage a continuous two part solution in which $f = 0$ for $\xi \geqslant 0$ and f is given by solving $(6.14)_2$ in the range $\xi < 0$. Equation $(6.14)_2$ can be integrated for integer $n \geqslant 3$ (Gradshetyn & Ryzhik 1965) to give

$$(n-1)S_1^{n-2}\xi = \begin{cases} \ln\left(\dfrac{S_1 - f}{S_1}\right) + \displaystyle\sum_{m=1}^{(n-2)/2} A_m + B_m & n \text{ even}, \\ \ln\left(\dfrac{S_1 - f}{S_1 + f}\right) + \displaystyle\sum_{m=1}^{(n-3)/2} A_m + B_m & n \text{ odd}, \end{cases} \tag{6.15}$$

where

$$\left.\begin{aligned} A_m &= \alpha_m \ln\left(\frac{S_1^2 - 2\alpha_m S_1 f + f^2}{S_1^2}\right), \\ B_m &= 2\beta_m\left\{\arctan\left(-\frac{\alpha_m}{\beta_m}\right) - \arctan\left(\frac{f - \alpha_m S_1}{\beta_m S_1}\right)\right\}, \end{aligned}\right\} \tag{6.16}$$

and

$$\alpha_m = \cos\left(\frac{2\pi m}{n-1}\right), \qquad \beta_m = \sin\left(\frac{2\pi m}{n-1}\right). \tag{6.17}$$

In general, this solution determines ξ as a function of the saturation f and it must be numerically inverted to give $f = f(\xi)$. However, for $n = 3$ there is no contribution from the summation term and the saturation is given explicitly by

$$f = \begin{cases} S_1\left(\dfrac{1 - \mathrm{e}^{2S_1\xi}}{1 + \mathrm{e}^{2S_1\xi}}\right), & \xi < 0, \\ 0, & \xi \geqslant 0. \end{cases} \tag{6.18}$$

This solution is illustrated in figure 3 for the far field saturations $S_1 = 0.25, 0.5, 0.75$

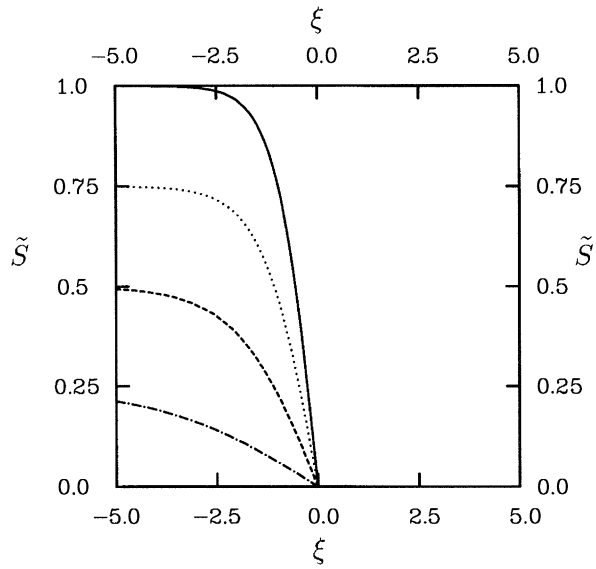

Figure 3. The class 2 travelling wave solution is illustrated for four different values of the far field saturation and exponent $n = 3$. The solid line corresponds to $S_1 = 1.0$, the dotted line to $S_1 = 0.75$, the dashed line to $S_1 = 0.5$ and the dot/dash line to $S_1 = 0.25$. Note the discontinuity in the solution at $\xi = 0$ and that the saturation is identically zero ahead of the front.

and 1.0. There is a finite gradient at $\xi = 0^-$ and zero gradient at $\xi = 0^+$. The snow ahead of the front is unaware that water is percolating through the snow until the front actually reaches that point which is physically more realistic than the class 1 solution. This class of models is, therefore, preferred to the structure presented in class 1.

(*c*) *Class 3*

The capillary pressure becomes unbounded, in the limit as the saturation tends to zero, when relations of the form (6.1) and (6.8) are used. This is not physically realistic. The approach of class 1 and 2 only succeeds in so far as another singularity $1/k^{\mathrm{rw}}$ was fortuitously introduced and controls the limit behaviour. In reality, a large but finite upper bound to the capillary pressure exists and is a requirement in more general models that seek to do more than predict the flow of water in a very special and restricted situation. (Recall that earlier we showed that these singularities necessarily lead to unbounded temperatures and phase change.)

This next class of problems represents a first step towards achieving a properly-posed theory, but as we shall see does not provide a complete remedy. Consider then an exponential capillary pressure relation in conjunction with the conventional relative permeability (3.7):

$$k^{\mathrm{rw}} = S_{\mathrm{e}}^{n}, \qquad p^{\mathrm{C}} = p_0 \exp(-rS_{\mathrm{e}}), \qquad n \geqslant 2, \tag{6.19}$$

where p_0 is the maximum capillary pressure, attained when $S_{\mathrm{e}} = 0$, and r is the decay rate. Some approximate magnitudes for these coefficients can be obtained by matching the value and gradient at some fixed saturation S_0 with the capillary pressure relation (3.10). Thus,

$$r = \frac{43}{S_0^2}\left(\frac{43}{S_0} + 380\right), \qquad p_0 = \left(\frac{43}{S_0} + 380\right)\exp(-rS_0), \tag{6.20}$$

which implies $r = 8.17$, $p_0 = 1759$ Pa for $S_0 = 0.074$ and $r = 158.2$, $p_0 = 1.95 \times 10^4$ Pa for $S_0 = 0.006$. Alternatively, we might suppose that the atmospheric pressure is a natural upper bound for the capillary pressure so $p_0 = 10^5$ Pa, and the decay rate

$$r = -\frac{1}{S_0} \ln\left[\frac{1}{p_0}\left(\frac{43}{S_0} + 380\right)\right] \tag{6.21}$$

equals 62.76 for $S_0 = 0.074$ or 430.67 for $S_0 = 0.006$. These estimates suggest that the maximum pressure lies in the range $10^3 \leqslant p_0 \leqslant 10^5$ Pa and the decay rate is in the range $5 \leqslant r \leqslant 500$.

Substituting the permeability and capillary pressure relations (6.19) into the saturation equation (5.3) yields

$$\phi^{\mathrm{e}} \frac{\partial S_{\mathrm{e}}}{\partial t} + \frac{1}{\gamma}\frac{\partial}{\partial z}\left(S_{\mathrm{e}}^n\right) = \frac{p_0 r}{\mu^{\mathrm{W}}/k}\frac{\partial}{\partial z}\left(S_{\mathrm{e}}^n \exp(-rS_{\mathrm{e}})\frac{\partial S_{\mathrm{e}}}{\partial z}\right), \tag{6.22}$$

where this time there is no cancellation between the permeability and capillary pressure gradients, so the right-hand side has a more complicated structure. Giving each term equal status determines the scales associated with the front:

$$t^* = \phi_{\mathrm{e}}^* \gamma z^* (S^*)^{1-n}, \qquad z^* = \chi\gamma S^* \exp(-rS^*), \tag{6.23}$$

where $\chi = p_0 r/(\mu^{\mathrm{W}}/k)$. To help in the comparison of the various cases we choose to correlate this length scale with that obtained in class 2, i.e. $z^* = 6$ cm, obtained using the power law (3.7) with exponent $n = 3$ at saturation $S^* = 0.074$. This implies that $r = 7.525$ and $p_0 = 1677$ Pa. Note that the timescale (6.23) has the same saturation dependence as those of classes 1 and 2, but the length scale has a very different behaviour. It suggests that for small saturation a decrease in S^* results in a steepening of the front, which is in direct contrast to the behaviour of the length scales in classes 1 and 2.

The non-dimensional saturation equation is obtained by substituting the scalings (6.23) and (5.7) into (6.22) to give

$$\tilde{\phi}^{\mathrm{e}} \frac{\partial \tilde{S}}{\partial \tilde{t}} + \frac{\partial}{\partial \tilde{z}}(\tilde{S}^n) = \frac{\partial}{\partial \tilde{z}}\left(\tilde{S}^n \exp(-\tilde{r}\tilde{S})\frac{\partial \tilde{S}}{\partial \tilde{z}}\right), \tag{6.24}$$

where the non-dimensional decay rate $\tilde{r} = rS^* \simeq 0.557$. We seek a travelling wave solution for uniform porosity of the form (6.5), and apply the boundary conditions $f \to S_1$ as $\xi \to -\infty$ and $f \to 0$ as $\xi \to +\infty$ to determine the front speed

$$v = S_1^{n-1}, \tag{6.25}$$

which is the same as in classes 1 and 2. The resulting ordinary differential equation for f:

$$-f(S_1^{n-1} - f^{n-1}) = f^n \exp(-\tilde{r}f)f', \tag{6.26}$$

has two solutions

$$f = 0, \qquad -(S_1^{n-1} - f^{n-1}) = f^{n-1}\exp(-\tilde{r}f)f'. \tag{6.27}$$

Once again solutions with a discontinuous derivative are permitted and we envisage a continuous two part solution in which $f = 0$ for $\xi \geqslant 0$ and for $\xi < 0$ f is given by solving $(6.27)_2$. An analytic solution for the case $n = 2$ is

$$\xi = \frac{1}{\tilde{r}}(1 - \exp(-\tilde{r}f)) - S_1 \exp(-\tilde{r}S_1)\int_{S_1 - f}^{S_1} \frac{\exp(\tilde{r}s)}{s}\,\mathrm{d}s, \tag{6.28}$$

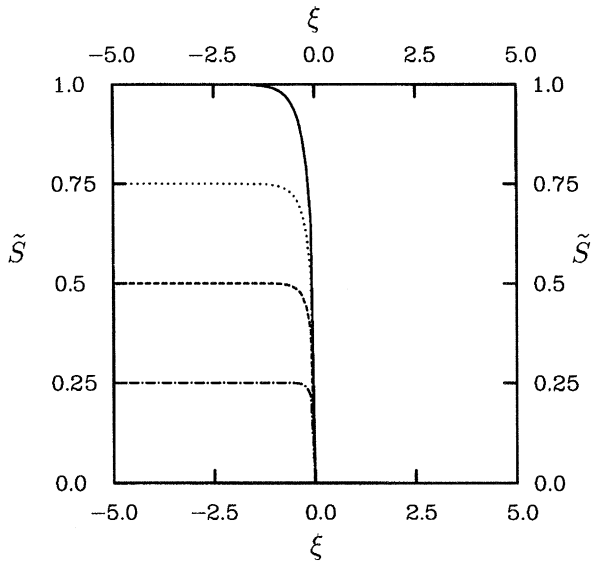

Figure 4. The class 3 travelling wave solution is illustrated for four different values of the far field saturation with exponent $n = 3$ and $\tilde{r} = 0.557$. The solid line corresponds to $S_1 = 1.0$, the dotted line to $S_1 = 0.75$, the dashed line to $S_1 = 0.5$ and the dot/dash line to $S_1 = 0.25$. The length scale associated with the front decreases with decreasing far field saturation and there is an infinite gradient at the origin. Note that the saturation is identically zero ahead of the front.

where the integral can be evaluated by expanding as a power series and interchanging the order of integration and summation. That is,

$$\int \frac{\exp(\tilde{r}s)}{s}\,\mathrm{d}s = \ln(s) + \sum_{m=1}^{\infty} \frac{\tilde{r}^m s^m}{m\,m!} + \text{const.} \tag{6.29}$$

The solution (6.28) is plotted in figure 4 for $\tilde{r} = 0.557$ and far field saturations $S_1 = 0.25$, 0.5, 0.75 and 1.0. The derivative discontinuity at $\xi = 0$ once again ensures that the snow ahead of the front is unaware of water percolating through the snow pack from above. However, there are two reasons why this model is rejected on physical grounds. Firstly, as the origin ($\xi = 0$) is approached from below, $f \to 0$ in $(6.27)_2$, and the derivative f' becomes unbounded. For low saturation, therefore, this solution behaves like a shock wave with an infinite gradient at the front. Secondly, the length scale associated with the front shortens as the saturation decreases. While this is simply a statement that finer scale features will be observed when the propagation speed is slower, we believe it to be physically unsatisfactory when it occurs in the limit as S^* tends to zero. These two observations are manifestations of the singular nature of the relative permeability (6.19).

(*d*) *Class 4*

Simply adopting a relation for p^{C} that keeps the capillary pressure bounded in the limit as the saturation tends to zero is not sufficient to construct a properly-posed theory. As the class 3 solutions have properties which are not physically realistic, such as steepening effects caused by the nonlinear diffusion decaying faster than the tendency for the wave to shock in the limit $S_{\mathrm{e}} \to 0$. However, if we ensure that the relative permeability has a finite gradient at $S_{\mathrm{e}} = 0$, then at very low saturation, the

nonlinear terms which are responsible for shocking are negligible, and low amplitude signals travel as a linear wave. We consider then an exponential permeability relation in conjunction with the exponential capillary pressure relation introduced in class 3:

$$k^{\mathrm{rw}} = \frac{\exp(cS_{\mathrm{e}}) - 1}{\exp(c) - 1}, \qquad p^{\mathrm{C}} = p_0 \exp(-rS_{\mathrm{e}}). \tag{6.30}$$

The relative permeability lies in the required range $0 \leqslant k^{\mathrm{rw}} \leqslant 1$ and the value of c may be approximated by correlating (6.30) and (3.7) at some fixed saturation S_0. This implies for $n = 2$ that $c = 5.63$ or 10.3, and for $n = 3$ that $c = 8.44$ or 15.4, with saturations $S_0 = 0.074$ or 0.006.

Recall that the saturation and velocity magnitudes for the power law permeability (5.7) were deduced from a balance between the gravitational and viscous drag terms (4.5). The new permeability relation (6.30) will be of magnitude $k^{\mathrm{rw}} \sim (\exp(cS^*) - 1)/(\exp(c) - 1)$ instead of $k^{\mathrm{rw}} \sim (S^*)^n$. It follows that when this is substituted into (5.6) the new mobile water saturation and velocity magnitudes are

$$S^* = c^{-1} \ln(1 + \gamma u_{\mathrm{w}}^* (\exp(c) - 1)), \quad v_{\mathrm{w}}^* = u_{\mathrm{w}}^* / \phi_{\mathrm{e}}^* S^*. \tag{6.31}$$

In order to draw comparisons between the two permeability relations (3.7) and (6.30) it is useful to choose $c = 7.516$ so that the saturation implied by (6.31) is $S^* = 0.074$, the same as for the power law with exponent $n = 3$ at the peak water flux $u_{\mathrm{w}}^* = 1.2 \times 10^{-6}\ \mathrm{m\,s^{-1}}$. With this c, it follows that $S^* = 0.0096$ at the lower flux $1.2 \times 10^{-7}\ \mathrm{m\,s^{-1}}$ which is about 3 times smaller than the saturation implied by the power law, so the water is moving faster at lower saturation. The corresponding velocity magnitudes are $v_{\mathrm{w}}^* = 3.2 \times 10^{-5}$ and $2.5 \times 10^{-5}\ \mathrm{m\,s^{-1}}$. Furthermore, there is a finite lower limit to the velocity magnitude as the water flux in (6.31) tends to zero

$$v_{\mathrm{w}}^* \longrightarrow \frac{c}{\phi_{\mathrm{e}}^* \gamma (\exp(c) - 1)} = 2.4 \times 10^{-5}\ \mathrm{m\,s^{-1}}. \tag{6.32}$$

This represents a *creep* state in which water continues to flow however low the saturation becomes, allowing complete drainage of the mobile water contained in the snow pack in finite time. This is a new model feature. Note, that a finite velocity magnitude v_{w}^* is consistent with the magnitudes $u_{\mathrm{w}}^* = 0$, $S^* = 0$ as $u_{\mathrm{w}}^* = \phi_{\mathrm{e}}^* S^* v_{\mathrm{w}}^*$ is still satisfied. This means that at very low saturation the water is able to move with a finite velocity whereas with the power law the velocity magnitude (5.7) decreases with decreasing water flux. In contrast to the exponential relation (6.30) the power law relative permeability would require an infinite time to elapse before complete drainage of the snow pack occurs. In § 8 the drainage properties of the two permeability relationships are discussed at greater length and some elementary numerical examples are presented.

Substituting the relative permeability and capillary pressure relations (6.30) into the saturation equation (5.3), and multiplying through by $(\exp(c) - 1)$, we obtain

$$\phi^{\mathrm{e}}(\exp(c) - 1)\frac{\partial S_{\mathrm{e}}}{\partial t} + \frac{1}{\gamma}\frac{\partial}{\partial z}(S_{\mathrm{e}}\kappa(S_{\mathrm{e}})) = \chi \frac{\partial}{\partial z}\left(S_{\mathrm{e}}\kappa(S_{\mathrm{e}}) \exp(-rS_{\mathrm{e}}) \frac{\partial S_{\mathrm{e}}}{\partial z}\right), \tag{6.33}$$

where the function

$$\kappa(S_{\mathrm{e}}) = (\exp(cS_{\mathrm{e}}) - 1)/S_{\mathrm{e}} \tag{6.34}$$

has a finite limit c as $S_{\mathrm{e}} \to 0$. It follows that (6.33) has a similar structure to the right-hand side of (6.9) in this limit. The length and timescales associated with the

front are

$$t^* = \phi_e^* \gamma (\exp(c) - 1) z^* \kappa^{-1}, \quad z^* = \chi \gamma S^* \exp(-rS^*). \tag{6.35}$$

The length scale takes exactly the same form as (6.23) in the class 3 solution, which appears to imply that the same steepening of length scales might occur in this case too. However, the creep state, at low saturation, prevents this as it allows water to propagate in linear waves which do not steepen to form shocks. That is, the length and timescales are those of the imposed (diurnal) forcing at the surface when the saturation is low and signals are transmitted as linear waves.

Applying the scalings (6.31) and (6.35) we obtain

$$\tilde{\phi}^e \frac{\partial \tilde{S}}{\partial \tilde{t}} + \frac{\partial}{\partial \tilde{z}} (\tilde{S} \tilde{\kappa}(\tilde{S})) = \frac{\partial}{\partial \tilde{z}} \left(\tilde{S} \tilde{\kappa}(\tilde{S}) \exp(-\tilde{r} \tilde{S}) \frac{\partial \tilde{S}}{\partial \tilde{z}} \right), \tag{6.36}$$

where

$$\tilde{\kappa}(\tilde{S}) = (\exp(\tilde{c}\tilde{S}) - 1)/\tilde{S}, \tag{6.37}$$

and $\tilde{c} = cS^*$, $\tilde{r} = rS^*$, which are both approximately equal to 0.557 for $S^* = 0.074$. Substituting a travelling wave solution of the form (6.5) for uniform porosity and applying the boundary conditions $f \to S_1$ as $\xi \to -\infty$ and $f \to 0$ as $\xi \to +\infty$ determines the front speed

$$v = \tilde{\kappa}(S_1), \tag{6.38}$$

and yields a differential equation

$$-f(\tilde{\kappa}(S_1) - \tilde{\kappa}(f)) = f \tilde{\kappa}(f) \exp(-\tilde{r} f) f', \tag{6.39}$$

with two solutions

$$f = 0, \qquad -(\tilde{\kappa}(S_1) - \tilde{\kappa}(f)) = \tilde{\kappa}(f) \exp(-\tilde{r} f) f'. \tag{6.40}$$

The same front speed v as that obtained for the power law relative permeability relation (6.6) at a given far field saturation, can be achieved by correlating (6.38) with (6.6) to show that $cS_1 = \log(1+S_1^n)$. For far field saturation $S_1 = 1.0$ this implies $c = \log 2 \simeq 0.693$. Note that as $\tilde{S} \to 0$ the function $\kappa(f) \to \tilde{c}$ and $\exp(-\tilde{r} f) \to 1$, so in the limit the gradient

$$f' \longrightarrow 1 - \tilde{\kappa}(S_1)/\tilde{c} \leqslant 0. \tag{6.41}$$

Moreover, if now the far field saturation S_1 tends to zero then the gradient at $\xi = 0^-$ also tends to zero, since $\kappa(S_1) \to \tilde{c}^+$. At low saturation the dominant balance lies between the terms on the left-hand side of the saturation equation (6.36) and the diffusion is an order of magnitude smaller, so the signals are transmitted as linear waves. It follows that the scaling argument above (6.35), which assumed there was always a balance between all three terms in (6.36), breaks down and the length scale does not shorten as the saturation tends to zero. A two part continuous solution to (6.40) exists in which $f = 0$ for $\xi \geqslant 0$ and f in the range $\xi < 0$ can be constructed numerically from the integral

$$\xi = -\int_0^f \frac{\tilde{\kappa}(s) \exp(-\tilde{r} s)}{\tilde{\kappa}(S_1) - \tilde{\kappa}(s)} \, \mathrm{d}s. \tag{6.42}$$

The saturation as a function of ξ is illustrated for the far field saturations $S_1 = 0.25$, 0.5, 0.75, and 1.0 in figure 5, with $\tilde{c} = 0.557$ chosen to give the same saturation at the peak water flux and $\tilde{r} = 0.557$ to give the same length scale as class 2, so direct

PHILOSOPHICAL TRANSACTIONS OF THE ROYAL SOCIETY A MATHEMATICAL, PHYSICAL & ENGINEERING SCIENCES

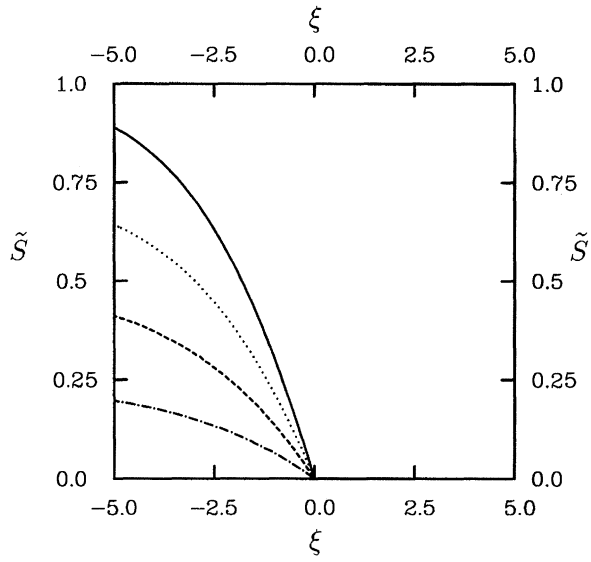

Figure 5. The class 4 travelling wave solution is illustrated for four different values of the far field saturation with $\tilde{c} = 0.557$ and $\tilde{r} = 0.557$. The solid line corresponds to $S_1 = 1.0$, the dotted line to $S_1 = 0.75$, the dashed line to $S_1 = 0.5$ and the dot/dash line to $S_1 = 0.25$. Note the discontinuity in the solution at $\xi = 0$ and that the saturation is identically zero ahead of the front.

comparison with figure 3 is possible. Increasing the value of $\tilde{r}$, illustrated in figure 6, steepens the front in the non-dimensional spatial coordinates, but can increase the physical length scale given by (6.35). Note, that the gradient at low saturations (6.41) is independent of $\tilde{r}$ and so the profile of the front can be made to look concave for larger $\tilde{r}$. In figure 7 the profiles for $\tilde{c} = 2.8$ and $\tilde{r} = 0.557$ show that increasing the value of $\tilde{c}$ also steepens the front. In this case the length scale remains the same as that in figure 5, but the timescale is reduced in (6.41). To make proper comparisons between each of the cases in physical coordinates, a universal time and length scale must be adopted: this is done later in § 8.

7. Numerical methods

In § 6 we discussed the appropriate scalings for four classes of permeability and capillary pressure relations and examined their relative merits by means of travelling wave solutions. We now turn our attention to constructing numerical methods to solve more general initial/boundary value problems associated with the non-dimensional saturation equations (6.4), (6.11), (6.24) and (6.36). These can be expressed in the general form

$$\tilde{\phi}^{\mathrm{e}} \frac{\partial \tilde{S}}{\partial \tilde{t}} + \frac{\partial}{\partial \tilde{z}}(F(\tilde{S})) = \frac{\partial}{\partial \tilde{z}}\left(G(\tilde{S}) \frac{\partial \tilde{S}}{\partial \tilde{z}}\right), \tag{7.1}$$

where the functions F, G for each class are summarized in table 2. An initial spatial distribution of the saturation, $\tilde{S} = \tilde{S}(\tilde{z})$, must be prescribed which includes the possibility that there is no mobile water content, $\tilde{S} \equiv 0$, in sections or in the whole of the snow domain. Two boundary conditions are then required to drive the model. The first of these is due to melt water infiltration at the surface of the snow where

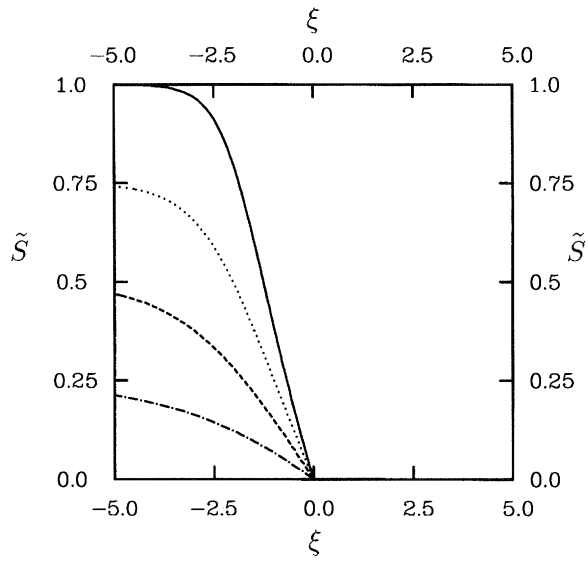

Figure 6. The class 4 travelling wave solution is illustrated for four different values of the far field saturation with $\tilde{c} = 0.557$ and $\tilde{r} = 2.0$. The solid line corresponds to $S_1 = 1.0$, the dotted line to $S_1 = 0.75$, the dashed line to $S_1 = 0.5$ and the dot/dash line to $S_1 = 0.25$. Note the discontinuity in the solution at $\xi = 0$ and that the saturation is identically zero ahead of the front.

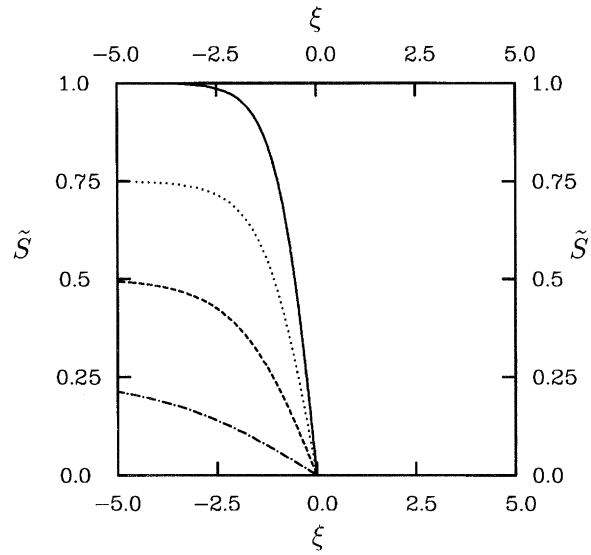

Figure 7. The class 4 travelling wave solution is illustrated for four different values of the far field saturation with $\tilde{c} = 2.8$ and $\tilde{r} = 0.557$. The solid line corresponds to $S_1 = 1.0$, the dotted line to $S_1 = 0.75$, the dashed line to $S_1 = 0.5$ and the dot/dash line to $S_1 = 0.25$. Note the discontinuity in the solution at $\xi = 0$ and that the saturation is identically zero ahead of the front.

either the saturation, its gradient, or some combination is prescribed. The second condition is a little more difficult. If the mobile water penetrates to the base of the pack, then the flow will either become saturated or travel laterally, and the second

Table 2. *Functional forms for each class of problems*

class	1	2	3	4	class 3 with change of variables
F	$\tilde{S}^n$	$\tilde{S}^n$	$\tilde{S}^n$	$\exp(\tilde{c}\tilde{S}) - 1$	$n^2(2n-1)^{-1}\sigma^{2-1/n}$
$F'(0)$	0	0	0	c	0
G	1	$\tilde{S}$	$\tilde{S}^n \exp(-\tilde{r}\tilde{S})$	$(\exp(\tilde{c}\tilde{S}) - 1)\exp(-\tilde{r}\tilde{S})$	$\sigma \exp(-\tilde{r}\sigma^{1/n})$
$G(0)$	1	0	0	0	0
$G'(0)$	0	1	0	c	1
H	—	—	—	—	$(1-n)n^{-1}\exp(-\tilde{r}\sigma^{1/n})$
$H(0)$	—	—	—	—	$(1-n)/n$

boundary condition arises from the complex coupling between the two regimes. Often the melt water waves never reach the base, as the surface forcing is not sustained for long enough, and so we assume here that the base of the snow lies in the far field where $\tilde{S} = 0$.

Solutions to nonlinear parabolic equations of the form (7.1) are obtained by using Newton's method (Smith 1985) to linearize the equations, and then iterating on an implicit tridiagonal matrix scheme until the corrections reach some pre-determined convergence criterion. This is indeed the best method for class 1 problems which are regular over the whole domain. However, classes 2–4 have a degenerate parabolic form, $G(0) = 0$, which support a discontinuous derivative at the moving boundary, $\tilde{z} = l(\tilde{t})$, between regions of non-zero and zero saturation. This method fails to represent this discontinuity properly and should only be applied when the saturation is non-zero throughout the whole pack domain. However, significant distortions are present only in the region close to the discontinuity, and reasonable accuracy has been achieved in reproducing the travelling wave solutions in the degenerate cases by this method. It may therefore be appropriate when only approximate results are required, or there is a complex structure with multiple moving boundaries.

An accurate numerical solution when a degenerate form describes the penetration into a region with no mobile water content is obtained by a fixed domain mapping technique originally developed by Morland (1982). We introduce the transformations

$$\zeta = l(\tilde{t}) - \tilde{z}, \qquad h = l(\tilde{t}), \tag{7.2}$$

so this moving boundary always lies at $\zeta = 0$; the snow surface now lies at $\zeta = h$ and h defines the depth of the melt front. Adopting (ζ, h) as independent variables in place of $(\tilde{z}, \tilde{t})$ the partial differential equation (7.1) becomes

$$\lambda\tilde{\phi}^{\mathrm{e}}\left(\frac{\partial\tilde{S}}{\partial h} + \frac{\partial\tilde{S}}{\partial\zeta}\right) - \frac{\partial}{\partial\zeta}(F(\tilde{S})) = \frac{\partial}{\partial\zeta}\left(G(\tilde{S})\frac{\partial\tilde{S}}{\partial\zeta}\right), \tag{7.3}$$

where

$$\lambda(h) = \frac{\mathrm{d}h}{\mathrm{d}t} \tag{7.4}$$

is the interface velocity. Note that the replacement of $\tilde{t}$ by the depth h as an independent variable requires that h is strictly monotonic in $\tilde{t}$. This means that the depth

PHILOSOPHICAL TRANSACTIONS OF THE ROYAL SOCIETY A MATHEMATICAL, PHYSICAL & ENGINEERING SCIENCES

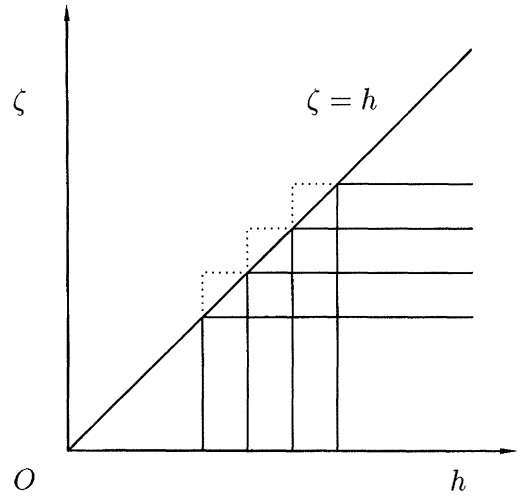

Figure 8. The snow surface lies along the 45° line $\zeta = h$ and the front lies at $\zeta = 0$ in the fixed domain (ζ, h). This ensures that the boundary conditions at the unknown moving boundary can be applied at grid nodes of a regularly spaced mesh.

of the melt front must be strictly increasing with time, which arises naturally in the present gravity flow theory. Equation (7.3) is subject to the boundary conditions

$$\left.\begin{aligned} \zeta = 0: &\quad \tilde{S}(0,h) = 0, \\ \zeta = h: &\quad \tilde{S}(h,h) \text{ is prescribed (say).} \end{aligned}\right\} \tag{7.5}$$

By (7.5), the depth rate of change $(\mathrm{d}\tilde{S}/\mathrm{d}h) = \partial\tilde{S}/\partial h = 0$ at the moving boundary $\zeta = 0$, so in the limit $\tilde{S} \to 0$ equation (7.3) implies that the interface velocity

$$\lambda(h) = \frac{1}{\tilde{\phi}^{\mathrm{e}}(\zeta = 0)} \left(F'(0) + G'(0) \left.\frac{\partial \tilde{S}}{\partial \zeta}\right|_{\zeta=0} \right), \tag{7.6}$$

and the time $\tilde{t}$ at which the melt front penetrates to depth d can then be computed from the integral

$$\tilde{t} = \int_0^{\mathrm{d}} \frac{1}{\lambda}\, \mathrm{d}h. \tag{7.7}$$

The snow pack configuration in (h, ζ) space is illustrated in figure 8; it occupies the lower triangular domain. Both the positions of the moving boundary $(\zeta = 0)$ and the snow surface $(\zeta = h)$ are known for each depth h, and so a regular discretization scheme, with uniform steps in ζ and h, ensures that all the boundary conditions are evaluated at a grid node. The nonlinear partial differential equation (7.3) does not degenerate in this fixed domain and can be solved, subject to the initial conditions, boundary conditions (7.5), and the consistency condition (7.6), by linearizing the equations and using an implicit tridiagonal scheme.

The fixed domain method works very well for classes 2 and 4, but fails for class 3. This is because finite λ in (7.6) implies that an unbounded saturation gradient must exist at the origin, since $G'(0) = 0$ and $F'(0) = 0$ in class 3. However, the singularity

can be removed by making the change of variables

$$\sigma = \tilde{S}^n, \tag{7.8}$$

and applying the transformations (7.2) to obtain

$$\lambda\tilde{\phi}^{\mathrm{e}}\left(\frac{\partial\sigma}{\partial h}+\frac{\partial\sigma}{\partial\zeta}\right)-\frac{\partial}{\partial\zeta}(F(\sigma))=\frac{\partial}{\partial\zeta}\left(G(\sigma)\frac{\partial\sigma}{\partial\zeta}\right)+H(\sigma)\left(\frac{\partial\sigma}{\partial\tilde{z}}\right)^2, \tag{7.9}$$

where the functions F, G and H for class 3 are given in table 2. This is very similar in structure to the saturation equation (7.3), but has an extra term on the right-hand side. The quantity σ does not change at the moving boundary and so we may deduce that the interface velocity is

$$\lambda=\frac{1}{\tilde{\phi}^{\mathrm{e}}(\zeta=0)}\left(F'(0)+\{G'(0)+H(0)\}\left.\frac{\partial\sigma}{\partial\zeta}\right|_{\zeta=0}\right). \tag{7.10}$$

This time $G'(0)$ and $H(0)$ are non-zero, so the gradient of σ is bounded at the interface and λ is properly defined. Equation (7.9) can therefore be integrated on the fixed domain where it does not degenerate, and the time can be computed from (7.7). Finally the saturation can be obtained by reversing the transformation (7.8).

8. Numerical illustrations

The numerical methods developed in § 7 are now applied to illustrate the differing responses of each class of model to simple forcing at the snow surface. In order to present a standard simulation where valid comparisons may be drawn, a universal time and length scaling based on class 2 with exponent $n = 3$ and saturation magnitude $S^* = 0.074$ is used. Equation (6.10) implies that $t^* = 2 \times 10^3$ s and $z^* = 6$ cm, which differ by a factor of 10 from the diurnal scales $t^{\mathrm{d}} = 2 \times 10^4$ s and $z^{\mathrm{d}} = 64$ cm. The basic simulation assumes that the initial saturation is identically zero throughout the snow pack and subsequently the snow surface saturation is prescribed as a function of time. The variation is chosen to be sinusoidal in time on the diurnal timescale t^{d}, so the boundary condition is

$$\tilde{S}(0,\tilde{t})=\sin\left(\frac{\pi t^*}{2t^{\mathrm{d}}}\,\tilde{t}\right), \tag{8.1}$$

where $t^{\mathrm{d}}/t^* \simeq 10$. Note that this does not necessarily imply that the same amount of mass enters the snow pack, as small capillary pressure gradients in the momentum balance introduce small perturbations to the flux entering the pack at any given time. The surface boundary condition (8.1) can be applied directly in the non-degenerate (class 1) solutions, but an iterative procedure must be used to ensure that the equivalent boundary condition $(7.5)_2$ in (ζ, h) space is evaluated at the correct time in the degenerate cases. In the non-degenerate case (class 1) the basal boundary condition $\tilde{S} = 0$ is applied at 20 non-dimensional space units (1.2 m in physical units of class 2), and in the degenerate cases no basal boundary condition is required as it is replaced by the condition $(7.5)_1$ at the interface. Note, that the class 1 equation is continuous for $\tilde{S}$ over the whole 20 spatial units while the degenerate case equations only extend to the depth of the front, so the total number of spatial grid points is always less for the fixed domain method and consequently runs much faster for the same grid spacing.

The universal class 2 length and timescalings are now formally applied. The saturation equation (5.3) has the basic form

$$\phi^{\mathrm{e}}\frac{\partial S_{\mathrm{e}}}{\partial t}+\frac{1}{\gamma}\frac{\partial}{\partial z}(\mathcal{F}(S_{\mathrm{e}}))=\frac{1}{\mu^{\mathrm{W}}/k}\frac{\partial}{\partial z}\left(\mathcal{G}(S_{\mathrm{e}})\frac{\partial S_{\mathrm{e}}}{\partial z}\right), \tag{8.2}$$

where the functions

$$\mathcal{F}(S_{\mathrm{e}})=k^{\mathrm{rw}}(S_{\mathrm{e}}),\quad \mathcal{G}(S_{\mathrm{e}})=-k^{\mathrm{rw}}(S_{\mathrm{e}})\frac{\mathrm{d}p^{\mathrm{C}}}{\mathrm{d}S_{\mathrm{e}}} \tag{8.3}$$

are dependent on the class of problem considered. The magnitudes F^*, G^* at a given saturation S^* are used to scale these functions and they are related to their non-dimensional counterparts by $\mathcal{F}(S_{\mathrm{e}})=F^*F(\tilde{S})$ and $\mathcal{G}(S_{\mathrm{e}})=G^*G(\tilde{S})$. When the class 2 time and length scales are used in the scalings (5.8) and (5.9) the non-dimensional saturation equation (8.2) becomes

$$\tilde{\phi}^{\mathrm{e}}\frac{\partial\tilde{S}}{\partial\tilde{t}}+D_t\frac{\partial}{\partial\tilde{z}}(F(\tilde{S}))=D_d\frac{\partial}{\partial\tilde{z}}\left(G(\tilde{S})\frac{\partial\tilde{S}}{\partial\tilde{z}}\right). \tag{8.4}$$

The non-dimensional number D_t is simply the ratio of the relative permeability of a given class to that of class 2, and D_d is simply the ratio of the diffusion coefficient of a given class to class 2, i.e.

$$D_t=F^*/(S^*)^3,\quad D_d=G^*/(43S^*). \tag{8.5}$$

Note that having the same time and length scales as those of class 2 in any given problem is equivalent to $D_t=1$ and $D_d=1$, respectively. For classes 1 and 3 the same power law relation is used for the relative permeability so $F^*=(S^*)^3$ and the timescales are the same automatically and $D_t=1$. There is no reliable data to determine the values of a_3 in (6.1) and p_0, r in (6.19), which would normally be used to set the value of D_d. Instead the natural length scale associated with class 2 is assumed to be an accurate representation of typical observed frontal length scales and we choose $D_d=1$. Thus, the length scales associated with classes 1 and 3 are chosen to be the same as class 2 by picking

$$a_3=43S^*/2,\quad p_0=43\exp(rS^*)/r(S^*)^2, \tag{8.6}$$

where, in the case of class 3, one free parameter r is left to alter the frontal properties. Class 4 has an exponential relative permeability, so the non-dimensional number

$$D_t=\frac{1}{(S^*)^3}\left(\frac{\exp(cS^*)-1}{\exp(c)-1}\right), \tag{8.7}$$

can only equal unity at saturation $S^*=0.074$ if $c=7.516$ ($\tilde{c}=0.557$). If the timescale is kept constant and another value of c is specified for the same peak water flux then a new saturation scaling follows from (6.31), e.g. $S^*=0.088$ for $c=9$ ($\tilde{c}=\log 2$). Alternatively, if the saturation remains at $S^*=0.074$ and $c=7.83$ ($\tilde{c}=\log 2$) then a different timescale is obtained and $D_t=0.771$. Finally, the same length scale as class 2 ($D_d=1$) can be ensured by picking

$$p_0=43S^*\exp(rS^*)\left(\frac{\exp(c)-1}{\exp(cS^*)-1}\right), \tag{8.8}$$

where both c and r are left as free parameters to control the wave speed, saturation and frontal properties. Unless otherwise stated the time and length scales are matched to those of class 2 by suitable choices of a_3, p_0, and $D_t=D_d=1$.

PHILOSOPHICAL TRANSACTIONS OF THE ROYAL SOCIETY A MATHEMATICAL, PHYSICAL & ENGINEERING SCIENCES

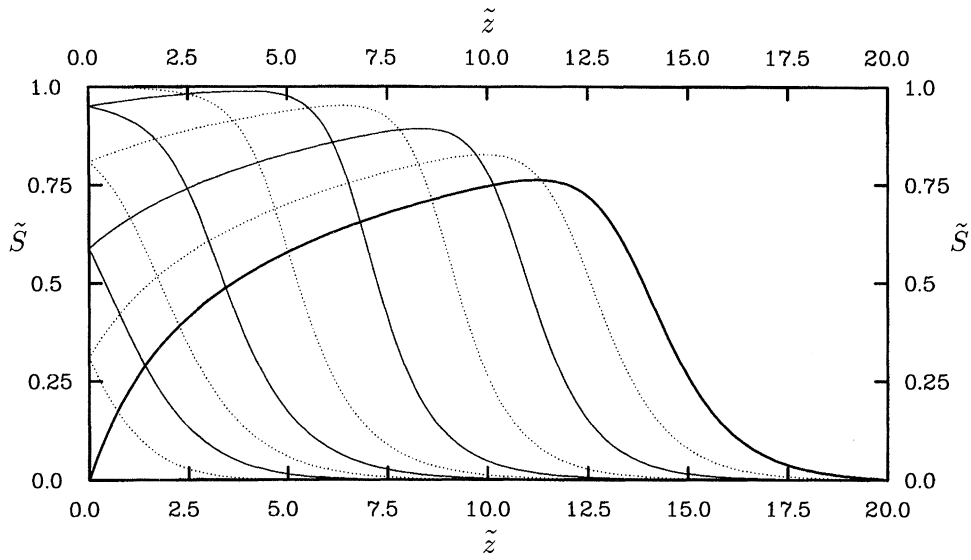

Figure 9. The saturation $\tilde{S}$ is plotted as a function of depth $\tilde{z}$ at intervals of two time units for class 1 with exponent $n = 3$. Initially the saturation was identically zero throughout the whole of the snow pack and then a sinusoidal variation in saturation was prescribed at the surface of the snow ($\tilde{z} = 0$) on a slow diurnal timescale. The first solution at $\tilde{t} = 2.0$ is illustrated with a dotted line and lies in the bottom left-hand corner, the next at $\tilde{t} = 4$ is illustrated with a solid line and this pattern is repeated until the final distribution at $\tilde{t} = 20$ is shown with the bold solid line. The solution is continuous over the entire snow domain.

During the day time solar radiation causes surface melt and the near surface saturation rises from zero to a maximum before returning to zero in the evening. Over night there is no surface melt and refreezing can take place. The surface boundary condition (8.1) used in the basic numerical simulation is representative of the melt water infiltration cycle during the day time, the surface saturation starts at zero at $\tilde{t} = 0$, rises to unity at $\tilde{t} = 10$ and decreases again to zero at $\tilde{t} = 20$. Note that in the final numerical solution the saturation is held at zero for a further 4 time units after $\tilde{t} = 20$ to demonstrate the drainage properties, at the onset of nightfall. Results are presented for each of the four classes and the saturation $\tilde{S}$ is plotted as a function of depth $\tilde{z}$ at intervals of two non-dimensional time units. The profiles for classes 1, 2 and 3 are illustrated in figures 9, 10 and 11, respectively. These are all reasonably similar in the expansion part of the wave profile behind the sharp interface, reflecting the low status of the diffusion term in the balance (5.3). The major differences occur at the front where the diffusion term approximately balances the nonlinear advection that is driving the formation of a shock. Each of the interface profiles, therefore, is very similar in form to the corresponding travelling wave front profiles illustrated in figures 1, 3 and 4. It is clear that relatively minor changes in the assumed functional form for the capillary pressure make a large difference to the solutions at the wave front. In class 1 the interface is smoothed so that it is continuous throughout the whole of the snow pack domain, so the saturation is dependent on the depth of the snow pack. While this does not significantly affect the solution in the example presented it would if the snow depth was halved, since the interface would have passed through the base of the pack and the basal boundary condition $\tilde{S} = 0$ would be violated. In class 2 the degenerate diffusive term allows

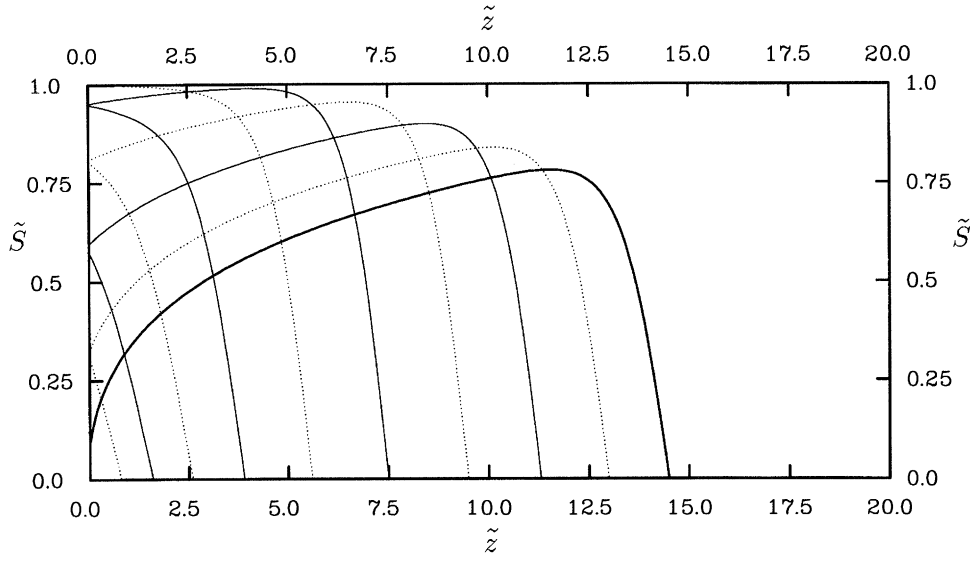

Figure 10. The saturation $\tilde{S}$ is plotted as a function of depth $\tilde{z}$ at intervals of two time units for class 2 with exponent $n = 3$. Initially the saturation was identically zero throughout the whole of the snow pack and then a sinusoidal variation in saturation was prescribed at the surface of the snow ($\tilde{z} = 0$) on a slow diurnal timescale. The first solution at $\tilde{t} = 2.0$ is illustrated with a dotted line and lies in the bottom left-hand corner, the next at $\tilde{t} = 4$ is illustrated with a solid line and this pattern is repeated until the final distribution at $\tilde{t} = 20$ is shown with the bold solid line. The solution has a discontinuity at the front ahead of which the saturation is identically zero. This is physically more realistic than class 1.

solutions with discontinuous derivatives and the snow ahead of the front is unaware that water is percolating through the snow pack above, which is physically more realistic. However, the capillary pressure has a singular behaviour at zero saturation which is not compatible with the theory of wet snow metamorphism. If the capillary pressure is chosen to remain bounded, as in class 3, then the solutions are similar, but the derivative becomes unbounded at the front. Not only is this physically unrealistic, but it presents considerable numerical difficulties in obtaining solutions. The problem stems from the $H(\sigma)(\partial\sigma/\partial\tilde{z})^2$ term in (7.9), and without investigating more accurate finite difference representations the change of variable method described in § 7 is not able to determine the velocity of the wave profile to sufficient accuracy. It has been found that the best solutions can actually be obtained by integrating the equivalent form,

$$\tilde{\phi}^{\mathrm{e}}\frac{\partial\tilde{S}}{\partial\tilde{t}} + \frac{\partial}{\partial\tilde{z}}(\tilde{S}^3) = \frac{-1}{\tilde{r}^4}\frac{\partial^2}{\partial\tilde{z}^2}(\exp(-\tilde{r}\tilde{S})\{\tilde{S}^3\tilde{r}^3 + 3\tilde{S}^2\tilde{r}^2 + 6\tilde{S}\tilde{r} + 6\}), \tag{8.9}$$

over the whole of the snow pack domain directly. As figure 11 demonstrates, degradation of the solutions only occurs close to the discontinuity in the derivative at the wave front.

The basic wave profile that develops is determined by the hyperbolic system obtained when the diffusive term is neglected. That is, for all three examples presented the equation

$$\tilde{\phi}^{\mathrm{e}}\frac{\partial\tilde{S}}{\partial\tilde{t}} + \frac{\partial}{\partial\tilde{z}}(\tilde{S}^3) = 0, \tag{8.10}$$

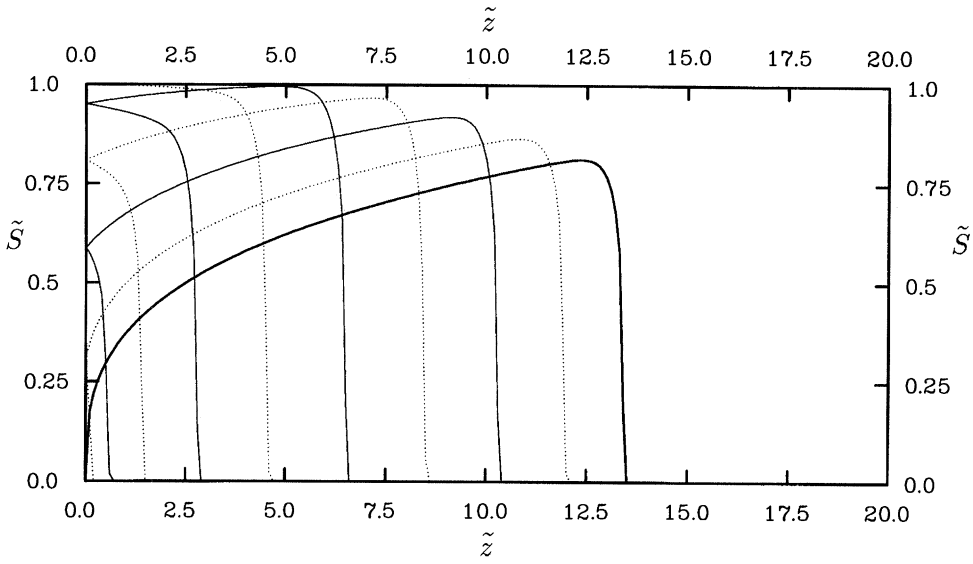

Figure 11. The saturation $\tilde{S}$ is plotted as a function of depth $\tilde{z}$ at intervals of two time units for class 3 with exponent $\tilde{r} = 0.557$. Initially the saturation was identically zero throughout the whole of the snow pack and then a sinusoidal variation in saturation was prescribed at the surface of the snow ($\tilde{z} = 0$) on a slow diurnal timescale. The first solution at $\tilde{t} = 2.0$ is illustrated with a dotted line and lies in the bottom left-hand corner, the next at $\tilde{t} = 4$ is illustrated with a solid line and this pattern is repeated until the final distribution at $\tilde{t} = 20$ is shown with the bold solid line. The solution has a discontinuity at the front ahead of which the saturation is identically zero.

which has been investigated by Colbeck (1972). In the loading phase as the saturation increases ($0 \leqslant \tilde{t} \leqslant 10$) a shock wave forms, and as unloading begins ($10 \leqslant \tilde{t} \leqslant 20$) the amplitude of the wave decreases. That is, a decrease in amplitude results from the hyperbolic nature of the equations and diffusion only plays a relatively minor role. Class 3 has the least diffusion of the three models and is therefore closest to the hyperbolic wave form. Class 2 and class 1 have progressively more diffusion and correspondingly slightly lower amplitudes. It is only in the non-degenerate class 1, where the diffusion is not reduced with decreasing saturation, that the smoothing effects dominate at very low saturation.

In class 4 the basic hyperbolic balance away from the sharp wave front is different to (8.10). At low saturation the creep state delays the time taken for the wave amplitude to decrease, since the relative velocity between high and low saturation is not as large as that with the power law and it takes longer for the wave form to shock. The class 4 solution with $\tilde{c} = 0.557$ and $\tilde{r} = 0.557$ is illustrated in figure 12, for which the corresponding travelling wave solution is illustrated in figure 5. Recall that the travelling wave speed is controlled by $\tilde{c}$ and that the value of 0.577 was chosen to correlate the relative permeabilities of the power law (3.7) and the exponential law (6.30) at peak saturation $S^* = 0.074$. Approximately the same total mass (i.e. the area under the saturation curve) enters into the snow, but the creep state slows down the shocking process so the amplitude remains higher for longer and there is much less skewing of the profile. In figure 12 the reduction in amplitude is in fact largely due to the relatively high amount of diffusion. The class 4 solution with the same $\tilde{c} = 0.577$ but increased $\tilde{r} = 2.0$, illustrated in figure 13, has much less

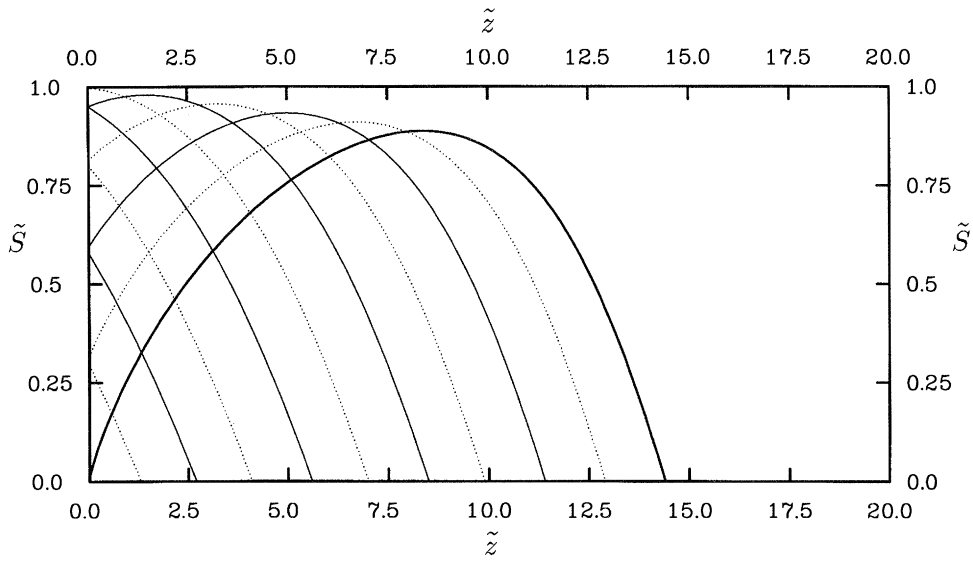

Figure 12. The saturation $\tilde{S}$ is plotted as a function of depth $\tilde{z}$ at intervals of two time units for class 4 with $\tilde{c} = 0.557$ and $\tilde{r} = 0.557$. Initially the saturation was identically zero throughout the whole of the snow pack and then a sinusoidal variation in saturation was prescribed at the surface of the snow ($\tilde{z} = 0$) on a slow diurnal timescale. The first solution at $\tilde{t} = 2.0$ is illustrated with a dotted line and lies in the bottom left-hand corner, the next at $\tilde{t} = 4$ is illustrated with a solid line and this pattern is repeated until the final distribution at $\tilde{t} = 20$ is shown with the bold solid line. This value of c was chosen so that the velocity is equal to that implied by the power law at the peak water flux u_{w}^{*}. Approximately, the same amount of water enters the pack but there is not as much skewing of the profile.

diffusion and the wave amplitude is barely decreased, while the steepness of the front is increased. It is possible to increase the rate at which the amplitude decreases with the exponential relative permeability relation by increasing $\tilde{c}$. This essentially makes the creep state slow down relative to the high saturation velocity so that the wave shocks faster. Figure 14 illustrates the class 4 solution with $\tilde{c} = 2.8$, $\tilde{r} = 0.557$ and with $D_t = 0.063$ and $D_d = 0.25$. The profile is almost identical to that obtained in class 2 with the power law. However, if the relative permeabilities are correlated this profile can only be achieved at higher saturation of magnitude $S^{*} = 0.311$. If amplitude decreases genuinely occur on the length scales suggested by the power law then the exponential relative permeability relation (6.30) is not general enough to reproduce these profiles in the correct parameter ranges. Figure 14 is indicative though that suitable relative permeability functions, perhaps low order polynomials, with finite gradients at $S = 0$ can be chosen to give the desired decay properties. In principal, then, functions may be found that maintain bounded capillary pressure, support a creep drainage, and can still produce profiles similar to those of class 2 illustrated in figure 10.

Finally, each of the models was run on to $\tilde{t} = 24$ time units with the surface saturation $\tilde{S}(0, \tilde{t}) = 0$ beyond the first cycle. Figure 15 illustrates that for the power law permeability present in classes 1, 2 and 3 the saturation can not decrease at the surface and the wave remains attached to $\tilde{z} = 0$. However, the creep state in class 4 allows a finite velocity in the limit as the saturation tends to zero and so the wave can detach from the surface. A moving boundary associated with a drainage front

PHILOSOPHICAL TRANSACTIONS OF THE ROYAL SOCIETY A MATHEMATICAL, PHYSICAL & ENGINEERING SCIENCES

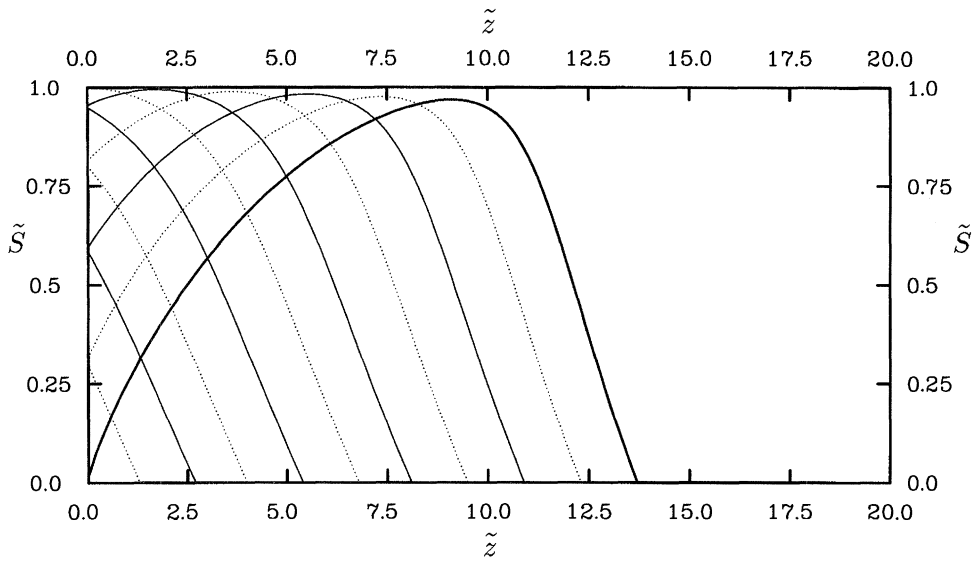

Figure 13. The saturation $\tilde{S}$ is plotted as a function of depth $\tilde{z}$ at intervals of two time units for class 4 with $\tilde{c} = 0.557$ and $\tilde{r} = 2.0$. Initially the saturation was identically zero throughout the whole of the snow pack and then a sinusoidal variation in saturation was prescribed at the surface of the snow ($\tilde{z} = 0$) on a slow diurnal timescale. The first solution at $\tilde{t} = 2.0$ is illustrated with a dotted line and lies in the bottom left-hand corner, the next at $\tilde{t} = 4$ is illustrated with a solid line and this pattern is repeated until the final distribution at $\tilde{t} = 20$ is shown with the bold solid line. This value of c was chosen so that the velocity is equal to that implied by the power law at the peak water flux u_{w}^{*}. The increased value of r results in greater skewing of the profile but less diffusion.

therefore penetrates into the snow pack, behind which the mobile water saturation is identically zero.

9. Discussion

This paper outlines the basic mixture theory for a phase-changing wet snow pack, which includes the small temperature variations due to curvature effects. The conservation balance laws are supplemented by constitutive postulates to obtain a closed system of equations. The conservation balances are presented in § 4 and an order of magnitude argument is used to show how selected terms can be neglected. Two further restrictions are needed to uncouple the saturation equation from the rest of the balances. These restrictions do not follow from the order of magnitude estimates made in § 4 and only apply in the special situation when there is no compaction of the ice matrix and no phase change. A situation which may be satisfied, to leading order, in the interior of a ripe pre-compacted snow pack. This simplified system of equations is used to demonstrate how the singularities introduced by the capillary pressure and the relative permeability can be removed, but in general the conservation balances of § 4 must be used.

The simplified saturation equation consists of three terms; a time rate of change term, a nonlinear advection term and a diffusion term. The diffusion term arises from the capillary effects and this prevents the formation of shocks, which occurs in the hyperbolic gravity flow theory of Colbeck (1972), replacing them instead by a sharp

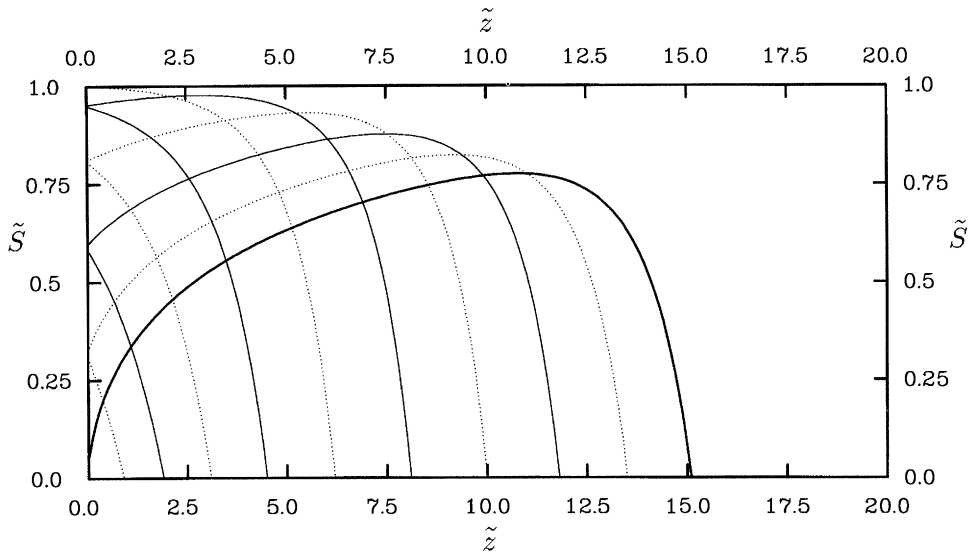

Figure 14. The saturation $\tilde{S}$ is plotted as a function of depth $\tilde{z}$ at intervals of two time units for class 4 with $\tilde{c} = 2.8$, $\tilde{r} = 0.557$ and $D_t = 0.063$, $D_d = 0.25$. Initially the saturation was identically zero throughout the whole of the snow pack and then a sinusoidal variation in saturation was prescribed at the surface of the snow ($\tilde{z} = 0$) on a slow diurnal timescale. The first solution at $\tilde{t} = 2.0$ is illustrated with a dotted line and lies in the bottom left-hand corner, the next at $\tilde{t} = 4$ is illustrated with a solid line and this pattern is repeated until the final distribution at $\tilde{t} = 20$ is shown with the bold solid line. The value of c was chosen to correlate the travelling wave front speed with that of the power law permeability. However, due to the nature of the boundary condition this allows more mass to enter the snow pack.

wave front with strong gradients. The characteristics of the front are dependent on both the relative permeability and the capillary pressure relation adopted. Away from the front the properties of the wave form are determined solely by the relative permeability relation. Earlier work (Colbeck 1974) has successfully reproduced observed run-off hydrographs, but, because of the singular nature of the capillary pressure at zero saturation, the model assumptions are not consistent with those in the theory of wet snow metamorphism. Wet snow models that model water movement and metamorphism will, therefore, encounter severe difficulties at low saturation and fail completely if the saturation reaches zero. Investigations into alternative capillary pressure relations, which remain bounded, demonstrate that to obtain physically satisfactory results the relative permeability must have a finite gradient as the saturation tends to zero. This introduces a creep state in which the water continues to flow however low the saturation becomes, allowing the snow pack to drain completely in finite time. The exponential relative permeability is a specific example of such a functional form. It can produce similar saturation profiles to those obtained with Colbeck's (1974) theory, but not for the correct parameter magnitudes. However, it is merely indicative that a suitable relative permeability relation, perhaps a low order polynomial, with the finite gradient property can be consistently applied in conjunction with the existing snow metamorphism theory.

This research has been supported by the Natural Environment Research Council. The formulation, analysis and presentation have all benefited from discussions with Professor L. W. Morland.

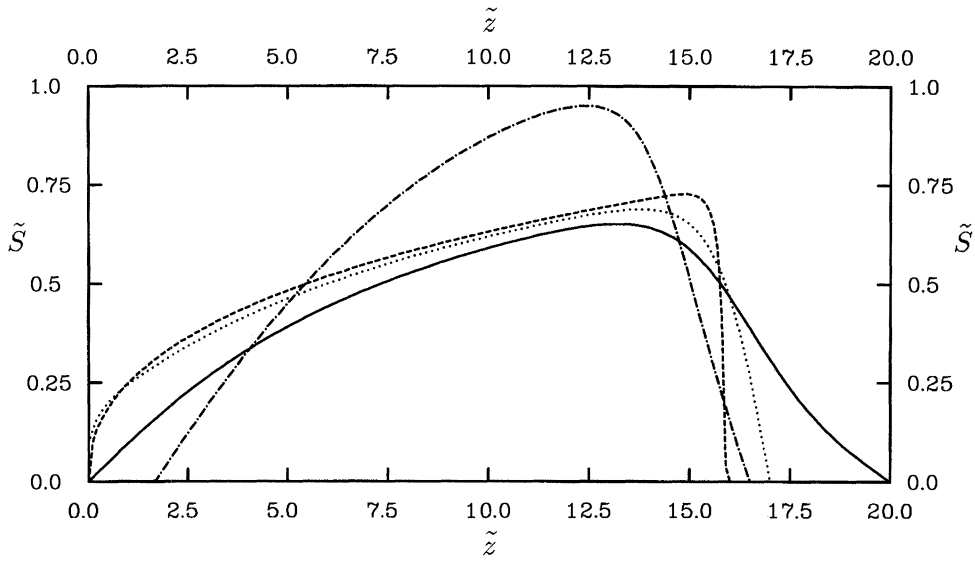

Figure 15. The saturation $\tilde{S}$ is plotted as a function of depth for class 1 (solid line), class 2 (dotted line), class 3 (dashed line) and class 4 (dot/dash line) at time $\tilde{t} = 24$. The sinusoidal forcing stopped at $\tilde{t} = 20$ and $\tilde{S} = 0$ has been applied at the snow surface $z = 0$ for the remaining four time units. The saturation profiles for classes 1, 2 and 3 are still attached to the snow surface, but the creep state allows the profile for class 4 to detach. Thus, complete drainage of the snow pack in finite time can only occur with the class 4 model.

References

Acheson, D. J. 1990 *Elementary fluid dynamics*. Oxford applied mathematics and computing science series. Oxford University Press.

Ambach, W., Blumthaler, M. & Kirchlechner, P. 1981 Application of gravity flow theory to the percolation of melt water through firn. *J. Glaciol.* **27**(95), 67–75.

Batchelor, G. K. 1967 *An introduction to fluid dynamics*. Cambridge University Press.

Bear, J. 1972 *Dynamics of fluids in porous media*. Elsevier.

Bengtsson, L. 1982 Percolation of meltwater through a snow pack. *Cold. Reg. Sci. Technol.* **6**, 73–81.

Colbeck, S. C. 1971 One-dimensional water flow through snow. CRREL Res. Rep., 296.

Colbeck, S. C. 1972 A theory of water percolation in snow. *J. Glaciol.* **11**(63), 369–385.

Colbeck, S. C. 1973 Theory of metamorphism of wet snow. CRREL Res. Rep., 313.

Colbeck, S. C. 1974 The capillary effects on water percolation in homogeneous snow. *J. Glaciol.* **13**(67), 85–97.

Colbeck, S. C. 1975 Grain and bond growth in wet snow. In *Snow Mechanics Symp. (Proc. Grindelwald Symp., April 1974*, vol. 114, pp. 51–61. IAHS-AISH

Colbeck, S. C. 1977 Short-term forecasting of water run-off from snow and ice. *J. Glaciol.* **19**(81), 571–588.

Colbeck, S. C. 1982 An overview of seasonal snow metamorphism. *Rev. Geophys. Space Phys.* **20**(1), 45–61.

Colbeck, S. C. 1987 A review of the metamorphism and classification of seasonal snow cover crystals. In *Avalanche Formation, Movement and Effects (Proc. Davos Symp., September 1986*, vol. 162, pp. 3–34. IAHS

Colbeck, S. C. 1989 Snow-crystal growth with varying surface temperatures and radiation penetration. *J. Glaciol.* **350**(119), 23–29.

Colbeck, S. C. & Anderson, E. A. 1982 The permeability of a melting snow cover. *Water Resources Res.* **18**(4), 904–908.

Colbeck, S. C. & Davidson, G. 1973 Water percolation through homogeneous snow. In *The Role of Snow and Ice in Hydrology (Proc. Banff Symp., September 1972*, vol. 1, pp. 242–257. Unesco WMO-IAHS

Gill, A. E. 1982 *Atmosphere–ocean dynamics*. International Geophysics series, vol. 30. Academic Press.

Gradshetyn, I. S. & Ryzhik, I. M. 1965 *Table of integrals, series, and products*. Academic Press.

Gray, D. H. 1980 The seasonal snowcover. In *Dynamics of snow and ice masses* (ed. S. C. Colbeck), pp. 305–395. Academic Press.

Gray, J. M. N. T. & Morland, L. W. 1994 A dry snow pack model. *Cold Reg. Sci. Technol.* **22**(2), 135–148.

Gray, J. M. N. T., Morland, L. W. & Morris, E. M. 1995 A phase changing dry snow pack model. *J. Glaciol.* **41**(137), 11–29.

Hobbs, P. V. 1974 *Ice physics*. Oxford University Press.

Jordan, R. 1991 A one-dimensional temperature model for a snow cover: technical documentation for SNTHERM. 89. *CRREL Special Rep.* **91-16**, 1–49.

Kuriowa, D. 1968 Liquid permeability of snow. Union de Géodésie et Géophysique Internationale, Association Internationale d'Hydrologie Scientifique. Assemblée générale de Berne, 25 Sept. – 7 Oct. 1967. (Commision de Nieges et Glaces.) Rapports et discussions, pp. 380–391.

Mellor, M. 1975 A review of basic snow mechanics. *Snow Mechanics Symp. (Proc. Grindelwald Symp., April 1974*, vol. 114, pp. 251–291. IAHS-AISH.

Morel-Seytoux, H. J. 1969 Introduction to flow of immiscible liquids in porous media. In *Flow through porous media* (ed. R. J. M. De Wiest). New York. Academic Press.

Morland, L. W. 1978 A theory of slow fluid flow through a porous thermoelastic matrix. *Geophys. J. R. Astr. Soc.* **55**, 393–410.

Morland, L. W. 1982 A fixed domain method for diffusion with a moving boundary. *J. Engng Math.* **16**, 259–269.

Morland, L. W. 1992 Flow of viscous fluids through a porous deformable matrix. *Surv. Geophys.* **13**, 209–268.

Morland, L. W., Kelly, R. J. & Morris, E. M. 1990 A mixture theory for a phase-changing snow pack. *Cold Reg. Sci. Technol.* **17**, 271–285.

Morris, E. M. & Godfrey, J. 1978 The European hydrological system snow routine. In *Proc. Modeling of Snow Cover Runoff* (ed. S. C. Colbeck & M. Ray), pp. 269–278. CRREL.

Scheidegger, A. E. 1960 *The physics of flow through porous media*. University of Toronto Press.

Smith, G. D. 1985 *Numerical solution of partial differential equations: finite difference methods*. Oxford applied mathematics and computing series, Oxford.

Wankiewicz, A. 1978 A review of water movement in snow. In *Proc. Modeling of Snow Cover Runoff* (ed. S. C. Colbeck & M. Ray), pp. 222–252. CRREL.

Weast, R. C. 1988 *Handbook of chemistry and physics*. Boca Raton, FL: CRC Press.

Whitham, G. B. 1974 *Linear and nonlinear waves*. Wiley–Interscience.

Received 10 May 1994; accepted 5 August 1995

PHILOSOPHICAL TRANSACTIONS OF THE ROYAL SOCIETY A MATHEMATICAL, PHYSICAL & ENGINEERING SCIENCES